Chemical Geology 572 (2021) 120196

Contents lists available at ScienceDirect

Chemical Geology

journal homepage: www.elsevier.com/locate/chemgeo

Diagenetic stability of non-traditional stable isotope systems (Ca, Sr, Mg, Zn) in teeth – An in-vitro alteration experiment of biogenic apatite in isotopically enriched tracer solution

Katrin Weber [a,*], Michael Weber [a], Martina Menneken [b], Anna G. Kral [b], Regina Mertz-Kraus [a], Thorsten Geisler [b], Jochen Vogl [c], Thomas Tütken [a]

[a] Institute of Geosciences, Johannes Gutenberg University, J.-J.-Becher-Weg 21, 55128 Mainz, Germany
[b] Institute of Geoscience, Rheinische Friedrich-Wilhelms University Bonn, Poppelsdorfer Schloß, 53115 Bonn, Germany
[c] Bundesanstalt für Materialforschung und -prüfung (BAM), Berlin, Germany

ARTICLE INFO

Editor: Dr. Oleg Pokrovsky.

Keywords:
Bioapatite
Isotopes
Raman spectroscopy
Diagenesis
LA-(MC-)ICP-MS
EPMA

ABSTRACT

Stable isotope ratios and trace element concentrations of fossil bones and teeth are important geochemical proxies for the reconstruction of diet and past environment in archaeology and palaeontology. However, since diagenesis can significantly alter primary diet-related isotope signatures and elemental compositions, it is important to understand and quantify alteration processes. Here, we present the results of in-vitro alteration experiments of dental tissues from a modern African elephant molar reacted in aqueous solutions at 30 °C and 90 °C for 4 to 63 days. Dental cubes with ≈ 3 mm edge length, comprising both enamel and dentin, were placed into 2 mL of acidic aqueous solution enriched in different isotopes (^{25}Mg, ^{44}Ca, ^{67}Zn, ^{86}Sr, initial pH 1). Element and isotope distribution profiles across the reacted cubes were measured with LA-(MC-)ICP-MS and EMPA, while potential effects on the bioapatite crystal structure were characterised by Raman spectroscopy. In all experiments isotope ratios measured by LA-(MC-)ICP-MS revealed an alteration of the enamel in the outer ≈ 200–300 µm. In contrast, dentin was fully altered (≈ 1.4 mm) after one week at 90 °C while the alteration did not exceed a depth of 150–200 µm during the 30 °C experiments. Then, the tracer solution started also to penetrate through the enamel-dentin junction into the innermost enamel, however, leaving the central part of the enamel unaltered, even after three months. The Raman spectra suggest an initial demineralisation in the acidic environment while organic matter (i.e. collagen) is still preserved. In the 90 °C experiment, Raman spectra of the $v_1(PO_4)$ band of the dentin shift over time towards synthetic hydroxylapatite patterns and the Ca (and Sr) concentrations in the respective solutions decrease. This indicates precipitation of newly formed apatite. Isotope and element concentration profiles across the dental tissues reveal different exchange mechanisms for different isotope systems. Magnesium is leached from enamel and dentin, while Zn is incorporated into the apatite crystal structure. However, the distribution of both elements is not affected in the innermost enamel where their concentrations do not change over the whole duration of the experiments. We found no correlation of reaction depth in the cubes and experimental duration, which might be caused by natural variability of the dental material already at the beginning of the experiment. Our alteration experiments in a closed system at high temperatures ≤90 °C and low initial pH demonstrate that at least the central part of mm-thick mammalian enamel apatite seems to be resistant against alteration preserving its pristine bioapatite mineral structure as well as its in-vivo elemental and isotopic composition. The experiments assess diagenetic alteration in a novel multi-proxy approach using in-situ analyses in high spatial resolution. It is demonstrated that the isotopes of Ca, Sr, Zn and Mg in the dentin are prone for diagenetic alteration, while enamel is more resistant against alteration and could be used for dietary and physiological reconstructions in fossil teeth.

* Corresponding author.
E-mail address: katrin.weber@uni-mainz.de (K. Weber).

https://doi.org/10.1016/j.chemgeo.2021.120196
Received 10 December 2020; Received in revised form 12 March 2021; Accepted 22 March 2021
Available online 26 March 2021

1. Introduction

Bones and teeth are important proxy archives for the reconstruction of diet, ecology, habitat use, and environment of extant and extinct vertebrates. Both traditional and non-traditional stable isotopes in bones and teeth have become important proxies for the reconstruction of diet ($\delta^{13}C$: e.g., DeNiro and Epstein, 1978; $\delta^{15}N$: DeNiro and Epstein, 1981), trophic level ($\delta^{44}Ca$: Skulan et al., 1997; Clementz et al., 2003; Heuser et al., 2011; Melin et al., 2014; Tacail et al., 2020; $\delta^{26}Mg$: Martin et al., 2014, 2015; $\delta^{66}Zn$: Jaouen et al., 2013, 2016a, 2016b, 2020; Bourgon et al., 2020; $\delta^{88/86}Sr$: Knudson et al., 2010; Lewis et al., 2017) and migration ($^{87}Sr/^{86}Sr$: Ericson, 1985; Price et al., 1994; Sillen et al., 1995; Hoppe et al., 1999), respectively. Environment- and diet-related element or isotope compositions are ingested from food and water and via metabolic processes incorporated into bones and teeth. Bones and teeth are hard tissues composed predominantly of bioapatite, a non-stoichiometric, carbonate-bearing hydroxylapatite with the formula $Ca_{10-x}[(PO_4)_{6-x}(CO_3)x]\ (OH)_{2-x}{\cdot}nH_2O$, where n ranges between 0.1 and 0.3 (Pasteris et al., 2014). The OH group in bioapatite is partly replaced by F, whereas Ca is partly substituted by, e.g., Mg, Zn, Sr, Na, and K due to their similar chemical behaviour and ion radii (e.g., Kohn et al., 1999; Boanini et al., 2010). Bone and tooth apatite is a complex solid solution that is further characterised by a small crystallite size on the order of 20 to 150 nm. Dental enamel has on average, larger bioapatite crystallites than bone and dentin, a significantly lower organic content (≈1%) of phosphoproteins and amelogenins, and negligible intrinsic porosity (Hillson, 2005). This makes tooth enamel much less prone to diagenetic alteration than bone and dentin, the latter which has similar properties as bone and is thus similarly susceptible to aqueous alteration and diagenetic changes (see overview in: Tütken and Vennemann, 2011). Due to its crystal-chemical properties, bioapatite is a highly reactive phase that, if its physical and chemical environment changes (for instance, after death of the individual), it has a high thermodynamic driving force to dissolve (Berna et al., 2004). In teeth, the organic and inorganic components vary significantly between different hard tissues such as enamel, dentin, and cement. While enamel contains about 960–990 mg/g hydroxylapatite, dentin and cement contain about 200 mg/g and ≈ 300 mg/g of collagen, respectively (Hillson, 2005). According to its different protein content, crystallite size, and porosity, enamel apatite is less vulnerable to diagenetic alteration than dentin and bone (Wang and Cerling, 1994; Hedges et al., 1995; Kohn et al., 1999; Hedges, 2002; Pfretzschner, 2004). Enamel, especially its trace element composition, can be altered during the fossilization process (e.g., Kohn et al., 1999; Schoeninger et al., 2003), while stable light isotope composition such as C and O (CO_3^{2-} or PO_4^{3-} group) are not prone to diagenetic alteration (Lee-Thorp et al., 1989, 2000; Ayliffe et al., 1994), except if microbes are involved (Zazzo et al., 2004a, 2004b).

Diagenetic alteration of the isotopic composition in bioapatite depends on several variables such as temperature, pH, chemical and isotopic compositions of the surrounding fluid and/or sediment as well as of the biogenic apatite itself. Some elements are more prone to diagenetic alteration than others, therefore every element or isotope system has to be checked for alteration individually. In general, systematic studies on the effect of diagenesis on trace element composition are rare. A good overview about the current knowledge of various isotope systems, such as Ca, Mg, Cu, Zn and Fe, as well as their diagenetic vulnerability in biological apatite and potential applications for vertebrate palaeobiology are given by Martin et al. (2017). Heuser et al. (2011) measured the calcium isotope composition of fossil dinosaur enamel as well as dentin from the same teeth and could not detect any diagenetic alteration of $\delta^{44/40}Ca$ values in both dental tissues, which was further supported by mass balance considerations. According to the negligible concentration of Ca in diagenetic fluids compared to the concentration of skeletal and dental tissue, Ca, unlike trace elements, should have a long-term preservation potential (Martin et al., 2017) However, especially trace elements, such as Sr, Mg and Zn, are more prone to diagenetic alteration compared to the major element Ca. A trace element study performed on Plio-Pleistocene South African australopithecine teeth displayed dramatically increased Zn levels in the fossil enamel samples, compared to Sr/Ca, Ba/Ca and Pb/Ca ratios, which were not significantly altered during fossilization (Sponheimer and Lee-Thorp, 2006). Different trace elements seem to be affected differently during diagenesis. Generally, the effect on Zn in fossil enamel seem to vary from site to site (Bocherens et al., 1994; Sponheimer and Lee-Thorp, 2006; Hinz and Kohn, 2010). Bourgon et al. (2020) measured enamel Zn isotope ratios of a diverse fossil Late Pleistocene fauna from the Tam Hay Marklot cave and found the $\delta^{66}Zn$ values still reflecting trophic level differences similar to modern mammals, supporting that the ante-mortem Zn isotope composition and concentration was still preserved. Both, in modern and fossil teeth they found the outermost enamel layer of <200 μm displaying higher Zn concentration. This Zn concentration increase towards the outermost enamel was also found in teeth of other large mammals and seems to be caused by the process of enamel maturation (Müller et al., 2019). Based on mass balance considerations a diagenetic Mg uptake seems to be unlikely, at least for terrestrial settings, since the Mg concentration in fresh water fluids (5–20 μg/mL, Shalev et al., 2017; Potasznik and Szymczyk, 2015) is negligible in comparison to the typical at least 100-fold higher Mg concentration in bioapatite (2000–10,000 μg/g, Martin et al., 2017). In contrast, because of the higher Mg concentration in seawater (~1300 mg/mL, Shalev et al., 2017), a diagenetic alteration of Mg in bioapatite deposited in marine settings is more likely. Overall, alteration of the trace element composition and isotope ratios can vary from one setting to another, according to the type of surrounding sediment, stratigraphic age as well as taphonomical and environmental conditions (e.g., Wang and Cerling, 1994; Kohn et al., 1999; Hedges, 2002). A study by Copeland et al. (2010) on Sr isotopes ($^{87}Sr/^{86}Sr$) in fossil rodent teeth from South Africa suggest little contamination of tooth enamel with diagenetic Sr, however, dentin was observed to have ≈ 50% diagenetic Sr. Another study by Budd et al. (2000) on archaeological human teeth also found a common, but highly variable diagenetic alteration of Sr in the dentin, potentially derived from the surrounding soil. Hoppe et al. (2003) demonstrate, that pretreatment can eliminate around 20% of diagenetic Sr from Holocene seal bones, and nearly 95% from fossil tooth enamel.

The understanding of alteration processes is paramount for the reconstruction of palaeoenvironmental or palaeodietary information from fossil teeth. However, still little is known about these processes and mechanisms driving those chemical and mineralogical alterations, such as recrystallication or isotope exchange processes. Thus far, only few diagenetic alteration experiments were made. Snoeck et al. (2015) performed an alteration experiment, where they put fragments of tooth enamel and calcined bones in ^{87}Sr-spiked solution for up to 1 year at room temperature and afterwards cleaned the samples using acetic acid washing and ultrasonic. $^{87}Sr/^{86}Sr$ was measured before and after the cleaning treatment, whereby all samples showed elevated ratios of $^{87}Sr/^{86}Sr$ before cleaning. After cleaning, only enamel remained significantly elevated in ^{87}Sr, indicating that porosity allows Sr to penetrate into the dental material, however, higher crystallinity of calcined bones in comparison to pristine bones and tooth enamel did not allow an incorporation of Sr into the crystal lattice. This is showing that apatite crystallinity plays a major role during diagenesis (Snoeck et al., 2015). There is only a small number of alteration experiments, dealing with the alteration of stable isotope compositions and apatite crystallinity changes. In most cases, alteration experiments are performed on bone material (e.g., Stiner and Kuhn, 1995; Berna et al., 2004; Pucéat et al., 2004; Munro et al., 2007; Kohn and Moses, 2013; Keenan and Engel, 2017; Aufort et al., 2019; Suarez and Kohn, 2020, Table S1). Berna et al. (2004) performed dissolution experiments in aqueous and buffered solution with synthetic hydroxylapatite and bone samples at 25 °C with the purpose of measuring the solubilities and therefore the stabilities of fossil bone under quasi-natural conditions. The so-called

recrystallisation window, the chemical conditions under which bone apatite can recrystallise into authigenic apatite, is restricted to a narrow pH range between 7.6 and 8.1. Preservation is best at a pH of above 8.1, whereby minerals will undergo recrystallisation in alkaline to neutral pH conditions. This, together with precipitation of additional apatite, will generally increase the crystallinity of the bone material. Berna et al. (2004) found, that under a pH of 7.5, the original bone mineral was totally recrystallised. An experiment on alligator bones buried in wetland soils and in experimental mesocosms with and without microbial colonization performed by Keenan and Engel (2017) found that this recrystallisation into a more stable apatite phase occurred already after one month of burial when microbial colonization was inhibited. Preservation of stable isotope compositions in bone were experimentally investigated by Munro et al. (2007) or Aufort et al. (2019). Munro et al. (2007) tested the effects of heating bone in air on the isotopic composition of phosphate oxygen, whereby the original $\delta^{18}O_{PO4}$ values were preserved at <300 °C and strongly shifts towards lower $\delta^{18}O_{PO4}$ values at higher temperatures, potentially due to ^{18}O exchanges with an external low-^{18}O reservoir in the phosphate oxygen. Whereas Aufort et al. (2019) performed immersion experiments of modern bones in aqueous NaF solution at pH 9–10 for up to three weeks at up to 70 °C and measured F, Ca and P concentrations, C and O isotopes, as well as vibrational (ATR-FTIR, Raman) and solid-state (H-1, C-13, F-19) NMR spectroscopies. They found a transformation mechanism by partial dissolution of biogenic apatite and precipitation of secondary apatite. There are only a few experiments on enamel hydroxylapatite (e.g., Koch et al., 1997; Zazzo et al., 2004a). Zazzo et al. (2004a) measured $\delta^{13}C$ and $\delta^{18}O$ of bone and tooth enamel powders after immersing the samples in ^{13}C- and ^{18}O-labelled water with the result of rapid and significant isotopic changes in the bone material, while tooth enamel is more resistant, however not exempt of alteration. Especially in the presence of microbial activity, even $\delta^{18}O_{PO4}$ values can alter in both, bone and tooth enamel. From the Raman spectroscopy perspective, spectra reveal modifications of the position and the full width at half maximum of the $v_1(PO_4^{3-})$ band caused by aqueous alteration (Thomas et al., 2007). In general, Raman spectroscopy is used in palaeontology for identification of mineralogical contents (Schweitzer et al., 1997), crystallinity changes (Person et al., 1995) and diagenetically induces ion concentration (MacFadden et al., 2010). Thomas et al. (2011) were able to detect io exchanges in apatite chemistry in fossil enamel and dentin samples indicating significant diagenetic alteration using Raman spectroscopy. They found Raman spectroscopy to be very useful a non-destructive tool for pre-screening fossil samples for diagenetic alteration (particularly CO_3^{2-}, F^- and Sr^{2+}).

To our knowledge, there are so far no experiments performed to assess the stability of original element and isotope compositions of enamel and dentin by exposing tooth pieces to aqueous solutions. The aim this study is to assess potential changes in chemical composition and crystal structure of the hydroxylapatite due to diagenetic alteration. Therefore, we present an extensive in-vitro alteration experiment assessing the stability of non-traditional stable isotopes against diagenetic alteration in enamel and dentin by immersing tooth pieces in an isotope tracer solution highly enriched in ^{25}Mg, ^{44}Ca, ^{67}Zn, and ^{86}Sr. These isotopes were chosen according to their relevance and increasing use as dietary and ecological proxies in palaeontology and archaeology (e.g., Knudson et al., 2010; Martin et al., 2014, 2015; Bourgon et al., 2020; Tacail et al., 2020). In theory, enamel should be highly resistant against diagenetic alteration, with minor or no changes in the chemical composition and crystal structure of the hydroxylapatite, while dentin should show alteration rather quickly. For this purpose, cubes cut from a modern elephant molar comprising both enamel and dentin were placed into the acidic tracer solution at 30 °C and 90 °C and for different time intervals (up to three months). The doped isotopes were highly concentrated in the experimental solution to enable us to easily trace the experimental post-mortem alteration of the original ante-mortem isotope composition. This experimental approach allows to assess the diagenetic stability of these non-traditional isotope systems used for dietary reconstruction and to characterise the physico-chemical mechanisms involved in tooth diagenesis. Changes of the chemical composition and isotopic composition in the reacted samples are measured in-situ with high spatial resolution using LA-ICP-MS, LA-MC-ICP-MS, electron microprobe and Raman spectroscopy on the dental cubes before and after the alteration experiments.

2. Material and methods

2.1. Dental material

A molar of a wild modern African elephant (*Loxodonta africana*) from Africa of unknown provenance (AG-Lox: Gehler et al., 2012) was cut into mm-sized dental cubes with a mean edge length of about 3.3 mm ± 0.3 mm (1SD) using a manual hand drilling device (Electer Emax NE129, Nakanishi Inc.). Due to practical reasons a modern elephant tooth was chosen, because of the thick layer of enamel compared to other mammals. This enabled us to analyse in-vitro induced alteration gradients in isotopic compositions along >1 mm long enamel profiles. Enamel thickness is on average 1.8 mm ± 0.2 mm (1SD), that of the dentin portion from the enamel dentin junction (EDJ) is on average about 1.4 mm ± 0.2 mm (1SD). The mean weight of the cubes was 63.8 mg ± 3.5 mg (1SD) (Table 1). An overview of the sampling locations on the dental cubes of the in-situ element and isotope analyses is provided in Fig. 1.

2.2. Isotope tracer solution

For all alteration experiments, an aqueous solution isotopically enriched in ^{25}Mg, ^{44}Ca, ^{67}Zn and ^{86}Sr was used (Table S2). The different isotopes ^{25}Mg, ^{67}Zn and ^{86}Sr (in HNO_3 solution) were mixed and evaporated at 80 °C down to a volume of ≈ 500 µL. ^{44}Ca was added (as carbonate powder, 34.8 mg $CaCl_2$, 97% ^{44}Ca) and evaporated at ≈ 55 °C to a volume of ≈ 100 µL. Afterwards 1 mL of $H_2^{18}O$ (Sigma-Aldrich, 97 atom-% ^{18}O) was added and the solution was filled up to 30 mL with D_2O (Sigma-Aldrich, 99.9 atom-% D). The final acidic tracer solution (pH of ≈ 1) was shaken and equilibrated for 3 h before entering the experiment. The element concentrations of the tracer solution after different time intervals of the dental immersion experiments and an aliquot of the starting solution were measured using a Thermo Element 2/XR ICP-MS system (University Bonn). Results are presented in Fig. 2 and Table S2.

2.3. In-vitro alteration experiment

The alteration experiments were performed in custom-made 3 mL Teflon beakers, self-sealed autoclaves with custom-made furnaces. The dental cube samples were weighted before and after the experiment to determine the weight loss. For each beaker, the temperature was constantly monitored during the experiment using a Digital Multimeter Voltcraft 840. Room temperature and relative humidity were monitored during the whole experiment, using a Tinytag Ultra 2 data logger – TGU-4500 (Gemini Data Loggers, Chichester, United Kingdom). The room temperature over the whole duration of the experiment was always below 26 °C (average 22.6 °C ± 2.0 °C). Each 3 mL Teflon autoclave was filled with 2 mL of aqueous tracer solution. One dental cube was added to each Teflon autoclave (Fig. 1). The experiments were carried out at 30 °C and 90 °C (± 1 °C) over a period of 4, 7, 14, 21 and 64 days (Table 1). After the experiment, the samples were washed three times with ultrapure water and dried in a desiccator for one day at room temperature. After drying, the samples were cut in half, perpendicular to the enamel-dentin junction (Fig. 1). On the first half, first LA-ICP-MS and LA-ICP-MC-MS measurements were performed, afterwards, after embedding and polishing, the same halves were used for Raman spectroscopy and electron microprobe measurement (Table S3). For further description of the embedding see section “Electron microprobe analysis” and “Raman spectroscopy”.

Table 1
Sample list of dental cubes with size and weight (before and after experiment).

Sample ID	Experiment	Temperature [°C]	Duration [days]	Length [mm]	Length after Experiment [mm]	Length loss [%]	Weight before Experiment [mg]	Weight after Experiment [mg]	Weight loss [%]
G	Isotopic tracer solution	30	4	3.52	3.42	2.8	59.5	49.1	17.5
K	Isotopic tracer solution	30	7	3.3	3.11	5.8	62	51.9	16.3
N	Isotopic tracer solution	30	14	3.25	2.91	10.5	64.8	54.6	15.7
C	Isotopic tracer solution	30	21	2.95	2.75	6.8	66.7	56.9	14.7
E	Isotopic tracer solution	30	64	3.14	2.91	7.3	66.8	56.5	15.4
A	Isotopic tracer solution	90	4	2.98	2.73	8.4	61.2	47.5	22.4
H	Isotopic tracer solution	90	7	3.17	2.81	11.4	62.9	48.2	23.4
I	Isotopic tracer solution	90	14	3.49	3.23	7.4	66.2	49.2	25.7
J	Isotopic tracer solution	90	21	3.01	2.86	5.0	67.8	52.9	22.0
F	Isotopic tracer solution	90	64	3.77	3.65	3.2	66.8	49.6	25.7
D	untreated reference sample	–	–	3.23			57.3	–	–
L	untreated reference sample	–	–	3.75			116.3	–	–
M	untreated reference sample	–	–	3.25			93.8	–	–

2.4. Laser ablation inductively coupled plasma mass spectrometry (LA-ICP-MS)

Trace element measurements were performed using an ArF Excimer laser system (193 nm wavelength, NWR193 by ESI/NewWave) equipped with a TwoVol^2 ablation cell and coupled to an Agilent 7500ce quadrupole ICP-MS (Agilent Technologies) at the Institute of Geoscience, University of Mainz. Laser repetition rate was set to 10 Hz. Line scans with a transition speed of 5 μm/s, using a fluence of 3.5 J/cm^{2}were carried out with a rectangular spot size of 130 μm × 30 μm. Pre-ablation was performed prior to each analysis to clean the surface. Background signals were acquired for 20 s during laser warm-up prior to each scan. ^{43}Ca was used as internal standard and synthetic NIST SRM 612 was used for calibration, using the preferred values from the GeoReM Database (Jochum et al., 2005). Data reduction was performed using an in-house Excel spreadsheet (Jochum et al., 2007). Details of the calculations are given in Mischel et al. (2017). For each day of measurement basaltic USGS BCR-2G and Durango Apatite were used as quality control materials to test accuracy and reproducibility of the measurements (Table S4). All reference materials were measured prior and after each sample block, three lines of 100 μm length respectively per reference material. Measured isotopes of interest are ^{24}Mg, ^{25}Mg, ^{26}Mg, ^{42}Ca, ^{44}Ca, ^{64}Zn, ^{66}Zn, ^{67}Zn, ^{68}Zn, ^{86}Sr and ^{88}Sr. The dental cubes were analysed prior to the experiment at the outer surface with one long line scan across the EDJ (start and end point beyond the cube). After the experiment, the freshly sawn surface was analysed in the same way, to determine the reaction depth of the solution into both dental tissues. The scans before and after the experiment differs slightly in length, since we measured on different plains of the same cube. The same untreated dental cube (cube D) was measured each time together with the altered cubes as reference cube to test the reproducibility and comparability between different measuring days (Table S5). Each line on this cube D was placed in close proximity to the previous one.

2.5. Laser ablation multi collector inductively coupled plasma mass spectrometry (LA-MC-ICP-MS)

In-situ analyses of Sr isotopes have been performed for all dental cubes after the experiment by LA-MC-ICP-MS. A first generation Nu Plasma MC-ICP-MS (Nu Instruments™) was coupled to a 213 nm Nd:YAG laser ablation system (New Wave Research™ UP-213) at the Max Planck Institute for Chemistry, Mainz, following the methods described by Weber et al. (2017, 2018). Data acquisition was performed in line scan analysis, covering the whole transect and across the EDJ. A circular spot size of 100 μm, a transition rate of 5 μm/s and a laser repetition rate of 10 Hz have been applied. Energy output was set to 100%, resulting in a fluence of 15–20 J/cm^2. Prior to each analysis, a pre-ablation of the sample surface was performed for cleaning purposes.

The following *m/z* ratios were monitored during analysis: 82, 83, 84, 85, 86, 87 and 88 and half masses 83.5, 85.5 and 86.5 (monitoring ^{167}Er, ^{171}Yb and ^{173}Yb, respectively) using time-resolved analysis (0.2 s integration time). To correct for Kr, we used the "on peak zero" method by measuring a 45 s gas background prior to each analysis without the laser firing (^{82}Kr < 0.2 m*V*). Calcium argide and dimer formation was found to be negligible by monitoring m/z 82 (<0.2 mV). Potential signals of doubly-charged REEs corrected by using constant isotope ratios for ^{167}Er and ^{171}Yb (Meija et al., 2016). To correct for the occurrence of ^{87}Rb on mass 87, we used the natural constant ^{87}Rb/^{85}Rb ratio of 0.3857 (Meija et al., 2016) and assume the same mass bias for Rb as for Sr. Mass bias correction was performed using the exponential law (Ingle et al., 2003) assuming a constant ^{86}Sr/^{88}Sr ratio of 0.1194. Strontium isotope analyses by LA-MC-ICP-MS can suffer from addition interferences on m/z 87 (ArPO and CaPO; e.g., Horstwood et al., 2008; Simonetti et al., 2008, Lewis et al., 2014; Lugli et al., 2017, Weber et al., 2020a). However, this effect is more pronounced for samples with low Sr concentration and did not affect our dental cube measurements. This is also visible in supplementary Fig. S1, where ^{87}Sr/^{86}Sr is plotted against 1/^{88}Sr [V] for the untreated dental cubes. If the interference of ^{40}Ca^{31}P^{16}O would affect the resulting ^{87}Sr/^{86}Sr, one would expect a strong linear correlation with increasing ^{87}Sr/^{86}Sr with increasing 1/^{88}Sr [V] (Horstwood et al., 2008; Lugli et al., 2017), which, however, is not the case.

Standard-bracketing was used as calibration protocol, applying the same laser parameters for the reference material and the samples (Irrgeher et al., 2016; Weber et al., 2017). An in-house marine shark tooth was used as reference material, using a modern-day seawater ^{87}Sr/^{86}Sr ratio of 0.70918 ± 0.00001 (McArthur et al., 2001) as reference value.

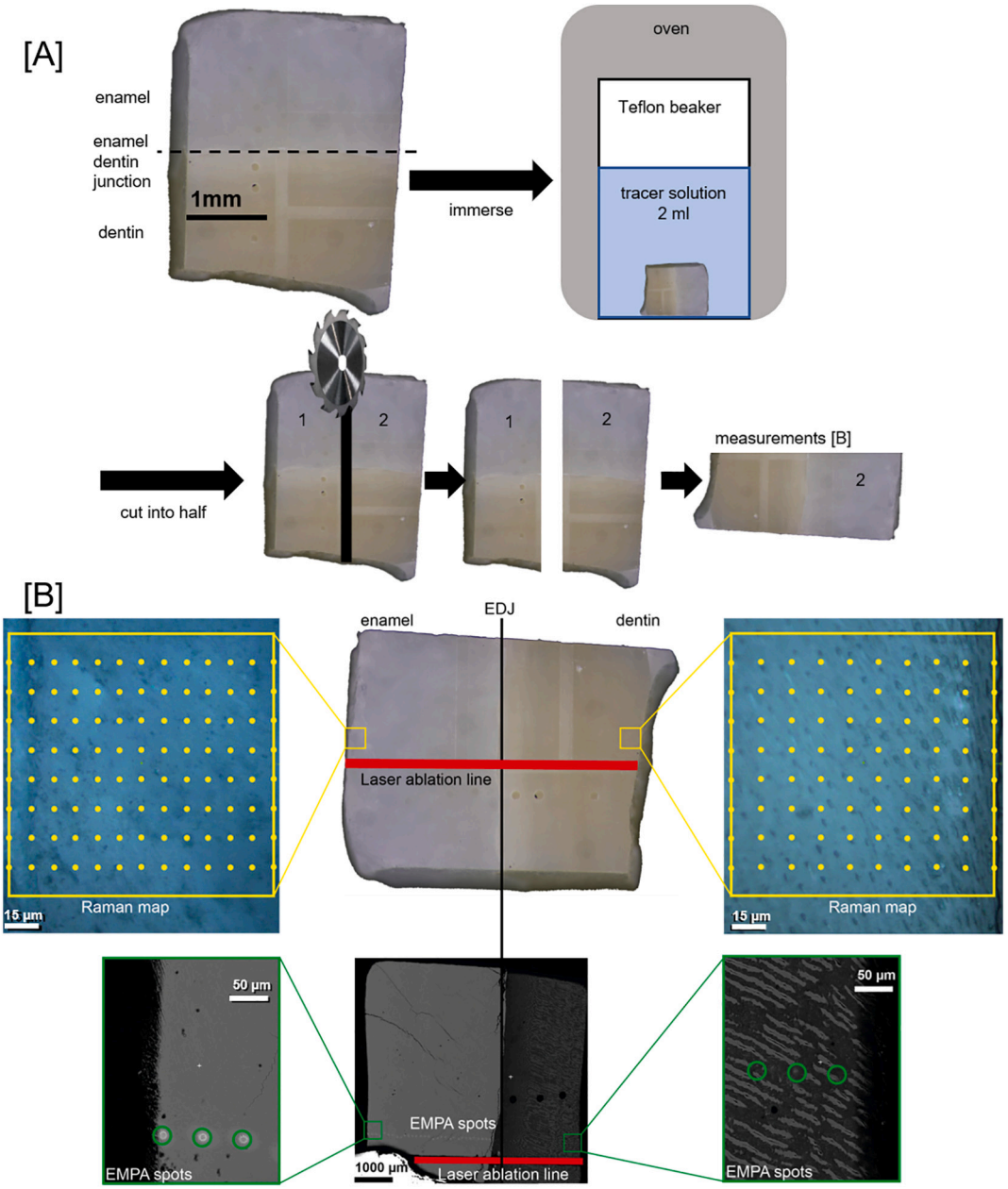

Fig. 1. A. Illustration of the experimental setup. Dental cubes, containing enamel and dentin, were immersed in isotopic tracer solution enriched in ^{25}Mg, ^{44}Ca, ^{67}Zn and ^{86}Sr in a Teflon beaker and heated in an oven. Afterwards the cubes were cut into half for in situ trace element and Sr isotope analysis. B. Illustration of the scans and maps measured with different in situ analytical techniques on the freshly sawn surface of one of the two halves of the dental cube. Red: Laser ablation lines of ICP-MS and MC-ICP-MS across the EDJ. Yellow: Raman maps, covering the outer 120 µm rim of both dental tissues, different number of rows for dentine ($n = 10$) and enamel ($n = 13$). Yellow dots indicate one Raman measurement respectively. Green: EMPA spots across EDJ, parallel to the laser ablation lines. (For interpretation of the references to colour in this figure legend, the reader is referred to the web version of this article.)

This is in the range of modern-day marine organisms (e.g., marine carbonate reference materials JCt-1 (giant clam, *Tridacna gigas*) and JCp-1 (coral, *Porites* sp.), yielding $^{87}Sr/^{86}Sr$ ratios of 0.709169 ± 0.000009 (2SE, $n = 3$) and 0.709170 ± 0.000006 (2SE, n = 3, Weber et al., 2018), respectively, and a modern Great white shark tooth having an average $^{87}Sr/^{86}Sr$ ratio of 0.709167 ± 0.000009 (2SE, $n = 10$, Vennemann et al., 2001).

Since the original tooth (AG-Lox) from which the dental cubes were processed is used as in-house reference material, additional analyses of the unaltered sample have been performed in the framework of further analyses, using a Neptune Plus MC-ICP-MS system (ThermoFisher Scientific) coupled with an ArF Excimer laser system (193 nm wavelength, NWR193 by ESI/NewWave) at the Institute of Geosciences, University of Mainz. All analyses using this system have been performed using a 500 µm long line scan, a transition speed of 5 µm/s and 0.262 s integration time. Due to different applications, the other laser parameters varied accordingly (spot size 70–110 µm, laser repetition rate 20–50 Hz and fluence of 3.5–5 J/cm^2). Data evaluation has been performed offline, using an in-house R-script, following the methods described below.

2.6. Laser ablation data processing

For calculation of the isotope ratios of interest, the background corrected raw data measurements obtained from the LA-(MC-)ICP-MS analyses were used.

The calculation was performed in a similar way for all isotope ratios

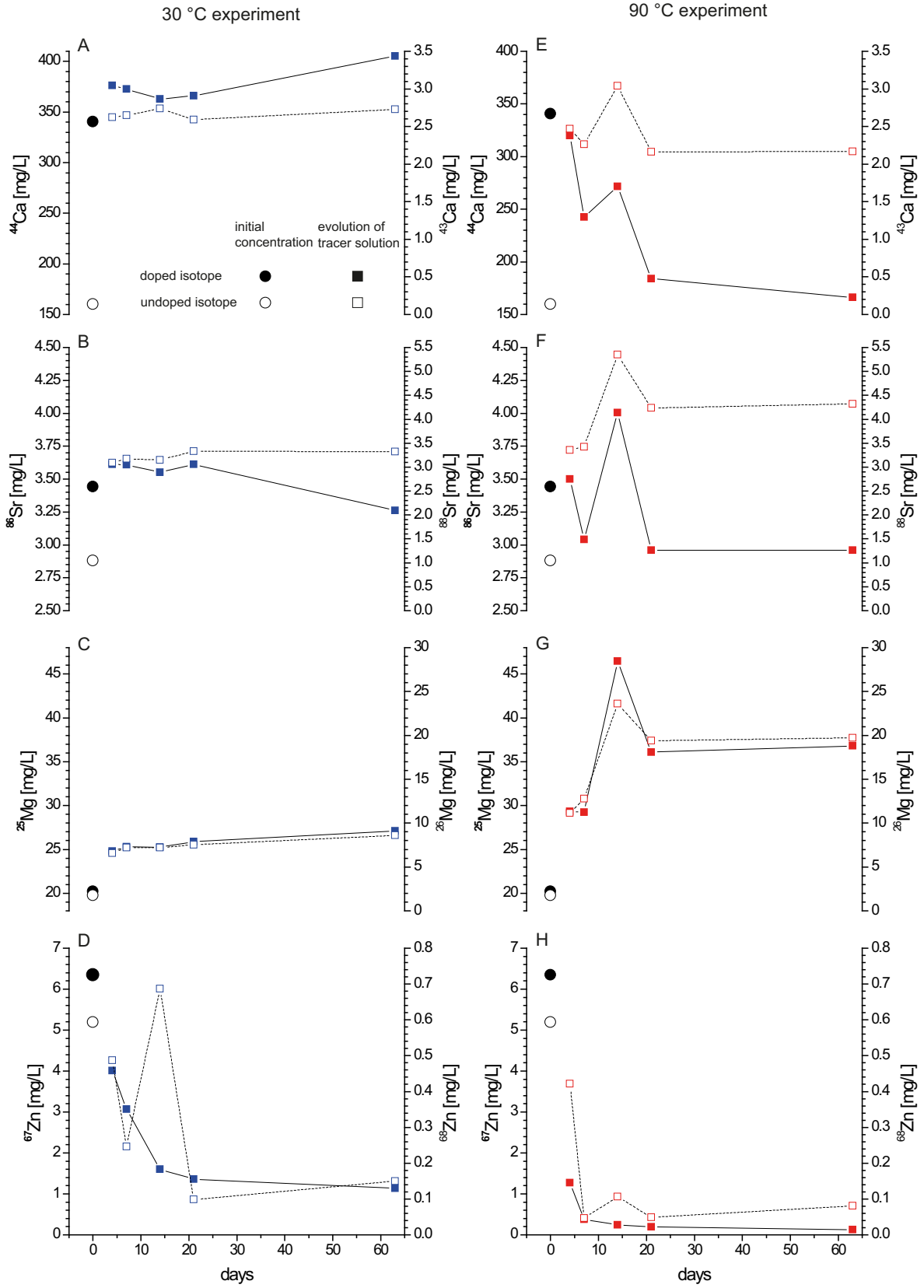

Fig. 2. Evolution of the doped isotopes in the isotopic tracer solution over the 30 °C (A–D) and 90 °C (E–H) experiment. Closed circles/rectangles indicate the concentration of the doped isotope (^{44}Ca, ^{86}Sr, ^{25}Mg, ^{67}Zn) in the solution, while open circles/rectangles represent the concentration of the undoped isotope (^{43}Ca, ^{88}Sr, ^{26}Mg, ^{68}Zn). The doped isotope are plotted against the primary axis, while the undoped isotope are plotted against the secondary axis. The initial concentration is represented as a black circle, the evolution during the 30 °C experiment is shown by blue rectangles and the 90 °C experiment by red rectangles. (For interpretation of the references to colour in this figure legend, the reader is referred to the web version of this article.)

and is therefore only described in detail once for the Sr isotope system as an example. The $^{87}Sr/^{86}Sr$ was chosen since it is widely used in geochemical studies of tooth enamel and dentin to determine habitat-use and migration patterns in palaeontology and archaeology (e.g., Clarke et al., 2007; Vroon et al., 2008). The $^{87}Sr/^{86}Sr$ was only corrected for mass bias and isobaric interference of Rb following the methods described for LA-MC-ICP-MS measurements in the section above.

Calculation of $^{44}Ca/^{42}Ca$, $^{25}Mg/^{24}Mg$ and $^{67}Zn/^{64}Zn$ ratios were performed similar to the $^{87}Sr/^{86}Sr$ using the exponential law for mass bias correction with the literature values for $^{42}Ca/^{44}Ca = 0.3102$, $^{24}Mg/^{26}Mg = 7.1728$ and $^{64}Zn/^{66}Zn = 1.7732$ (Meija et al., 2016). Isobaric interferences affecting Mg, Ca and Zn (e.g., Galy et al., 2001; Wieser et al., 2004; Zhu et al., 2015) were not corrected for the LA-ICP-MS data. Then a 100-point running mean was calculated for all isotope ratios.

To evaluate if there are alteration effects on the element concentration independent or dependent on the isotope of interest for the respective element, i.e., doped vs. un-doped isotope, ^{n}element/Ca ratios (e.g., $^{86}Sr/Ca$ vs. $^{88}Sr/Ca$) have been calculated, with n = mass number of the specific isotope. For undoped samples, those ratios are expected to be identical, while doped parts should yield diverging results.

2.7. Solution MC-ICP-MS analysis

To further evaluate the initial isotopic values of Sr ($^{87}Sr/^{86}Sr$) and Ca ($^{44}Ca/^{42}Ca$ expressed as $\delta^{44/42}Ca$) of the original dental material (AG-Lox) solution-based MC-ICP-MS analyses have been performed on enamel bulk powder samples. Purification of Sr and Ca has been performed using a prep*FAST* MC (ESI Elemental Scientific) using a 1 mL Sr-Ca ion chromatographic column following the default Sr-Ca separation protocol. Strontium isotopes were measured in 0.8 mol/L distilled HNO_3 following the methods described by Weber et al. (2018), using a Neptune Plus MC-ICP-MS coupled with an Aridus3 (CETAC Technology) at the Institute of Geosciences, University of Mainz. NIST SRM 987 (Strontium carbonate isotopic standard) was used as reference material for standard bracketing (long-term $^{87}Sr/^{86}Sr = 0.710279 \pm 0.000027$ (1SD, n = 506) and normalizing measured values to a commonly accepted $^{87}Sr/^{86}Sr$ of 0.710248 (McArthur et al., 2001). Calcium isotope analyses were performed in 0.5 mol/L distilled HNO_3 following the protocol of Tacail et al. (2014), using a Neptune Plus MC-ICP-MS coupled with an Apex Omega HF (ESI Elemental Scientific) at the Institute of Geosciences, University of Mainz. An Alfa Aesar plasma standard solution (Lot.Nr. 8,142,996) was used as reference material for standard bracketing of the Ca isotope ratio. The $\delta^{44/42}Ca$ was calculated relative to NIST SRM 915a using IAPSO and NIST SRM 1400 reference materials. Sample solutions have been prepared to match the concentration of the reference solution within 10% (10 µg/L for Sr, 2 mg/L for Ca).

2.8. Raman spectroscopy

For Raman spectroscopic measurements, the same halves of the dental cubes were embedded in the fast hardening resin Technovit 5071 and polished. The measurements were performed at the Institute of Geoscience, University of Bonn, using a Horiba Scientific HR800 confocal Raman equipped with an Olympus BX41 microscope and an electron-multiplier CCD detector. A 200 mW, 784 nm diode-pumped solid-state laser was applied as excitation source. A 50 times objective with a numerical aperture of 0.75 and a confocal hole of 1000 µm were used for all measurements, resulting in a theoretical, diffraction limited lateral and axial resolution on the order of about 1.3 and 5.5 µm, respectively. The scattered light passed a 100 µm spectrometer entrance slit and was dispersed by a grating with 600 grooves/mm. The 520.7 cm^{-1} line of a silicon standard was used for initial calibration of the spectrometer, while the 985.43 cm^{-1} line of a neon lamp (Saloman, 2006) was used as an internal standard to be able to correct for any spectrometer shift occurring during analysis by placing a Ne lamp alongside the beam path of the scattered light. The 520.7 cm^{-1} line of a silicon standard was used for initial calibration, while the 985.43 cm^{-1} Ne line was then used as an internal standard to correct for any linear shift occurring during analysis, e.g., due to small temperature fluctuation in the laboratory (±0.5 °C). With these settings, the spectral resolution was 2.478 ± 0.006 cm^{-1} as estimated from the width of the Ne line. Point-by-point measurements were performed with an acquisition time of 60 s and three accumulations per point in the frequency range between 360 and 1200 cm^{-1} for enamel and between 750 and 1450 cm^{-1} for the dentin, due to the different structures of enamel and dentin. With 10 spots parallel to the cubes edge and 10 (dentin) and 13 (enamel) spots into the sample, an area of 120 × 120 μm^2 was covered for all samples. To observe changes in crystallinity of the hydroxylapatite or potential incorporation of isotopes from the tracer solution the $v_1(PO_4)$ symmetric stretching band near 960 cm^{-1} of apatite was fitted using the LabSpec 6 program of Horiba Scientific. In case of isotope incorporation shifts in $v_1(PO_4)$ band position and width (e.g., Thomas et al., 2011). In all samples a slight asymmetry of the $v_1(PO_4)$ band was observed. To quantify changes in the width Γ (given as full width at half maximum, FWHM) and frequency of the $v_1(PO_4)$ band, an asymmetric Gauss-Lorentz function was used. All other bands were fitted with symmetric Gauss-Lorentz function along with a linear background function between 900 and 1200 cm^{-1}. Furthermore, finite slit width effects on the width of the Raman bands were corrected using the following equation (Tanabe and Hiraishi, 1980):

$$\Gamma_c = \Gamma_m \left[1 - (S/\Gamma_m)^2\right]$$

with Γ_m and Γ_c representing measured and corrected bandwidth, respectively, and S the spectra resolution (= 2.478 cm^{-1}).

2.9. Electron microprobe analysis

For electron microprobe analysis (EMPA), the halves of the dental cubes (already embedded in Technovit) were further embedded in epoxy resin, polished, cleaned and sputtered with a ≈ 20 nm layer of carbon. Experimentally altered dental cubes were solely measured after the experiment, together with untreated samples D, L and M (Table 1). Analyses were carried out at the Institute of Geosciences, University of Mainz, using a Jeol JXA 8200 electron microprobe in wavelength-dispersive spectrometry (WDS) mode. A beam current of 12 nA and an acceleration potential of 15 kV were chosen, with the electron beam defocused to 10 µm. Peak counting times were 30 s for Ca, P and Mg, 120 s for Zn and 80 s for Sr. Raw element concentration data were corrected using the routine by Armstrong (1995) and an in-house apatite reference material was chosen for calibration. A profile of 10 µm spot measurements with a distance of 40 µm between the spot centres was analysed across the enamel thickness across the EDJ into to the dentin (Fig. 1).

3. Results

3.1. Changes in physical properties of the dental cubes

All dental cubes become very brittle during the preparation after immersion in the tracer solution at 90 °C, indicating higher porosity, especially sample I (14 days, 90 °C) shows a clear dissolution of dentin, especially at the boundary to the enamel (Fig. S2). All cubes have a few µm-thick, pale whitish coating on the dental surface, which was too thin to be detected in the different measurement methods used in this study. All cubes have a weight loss of around 15.5 % ± 1.5 % (30 °C) and 23.5 % ± 2.3 % (90 °C), which is also reflected in an average size decrease of the dental cubes leading to an average length loss (length across enamel dentin junction) of 6.6 % ± 2.5 % (30 °C) and 7.1 % ± 2.8 % (90 °C), respectively.

3.2. Tracer solution composition

The pH value of the solution rose by the first week of experiment from pH ≈ 1 to pH ≈ 6–7 and stayed relatively constant throughout the remaining experiment. The evolution of the elemental and isotopic composition of the tracer solution is shown in Fig. 2 and Table S2.

3.2.1. Calcium

The Ca of the raw tracer solution consisted almost purely of the doped isotope ^{44}Ca (340 mg/L, Fig. 2A, E), while the ^{43}Ca content was almost negligible (0.14 mg/L, Fig. 2 A, E). During the 30 °C experiment, ^{44}Ca increased up to 376 mg/L after four days and remained rather constant and only increased up to 405 mg/L after 63 days. A contrasting evolution is visible during the 90 °C experiment, where ^{44}Ca decreased (nearly exponential, apart from cube I, 14 days, see Fig. S2) in the tracer solution during the whole experiment down to a concentration of 166 mg/L after 63 days. The undoped ^{43}Ca shows a similar behaviour for both experiments, with a strong initial increase towards 2.62 mg/L (30 °C) and 2.47 mg/L (90 °C), with almost constant concentrations afterwards (apart from cube I, 14 days, 90 °C, see above).

3.2.2. Strontium

In comparison to the other used element solutions enriched in a specific isotope, the ^{86}Sr-enriched solution was not as pure and also contained a significant amount of ^{88}Sr. Therefore, the tracer solution has ^{86}Sr (3.44 mg/L, Fig. 2B, F) and ^{88}Sr (1.05 mg/L, Fig. 2 B, F). Overall, the Sr concentration in the solution displays a similar behaviour as Ca. For the 30 °C experiment, a slight increase in the ^{86}Sr is visible after four days (3.61 mg/L), which then remains almost constant, except for a small decrease after 63 days (3.26 mg/L). During the 90 °C experiment, the ^{86}Sr concentration decreases over the experimental duration (except for cube I, 14 days, 90 °C) down to 2.96 mg/L after 63 days (Fig. 2F). This decrease is not as strong as for Ca, however, the general trend is similar. The ^{88}Sr increases already after four days of experiment up to 3.09 mg/L (30 °C) and 3.36 mg/L (90 °C) and increases slightly over time (Fig. 2 B, F).

3.2.3. Magnesium

The evolution of the Mg concentrations is almost identical for both analysed isotopes and at the two different temperatures (Fig. 2C, G). Both, the doped ^{25}Mg (24.8 mg/L 30 °C and 29.3 mg/L 90 °C), as well as the undoped ^{26}Mg (6.6 mg/L 30 °C and 11.1 mg/L 90 °C), increase significantly after four days in comparison to the starting solution (^{25}Mg 20.2 mg/L and ^{26}Mg 1.8 mg/L). Afterwards, the concentration for both Mg isotopes increases slightly during the experimental period. In addition, the concentration increases strongly during the 90 °C experiment.

3.2.4. Zinc

The evolution of Zn in the tracer solution is similar for both isotopes and temperatures (Fig. 2D, H). While the raw solution has the highest concentration for the doped ^{67}Zn (6.35 mg/L) and undoped ^{68}Zn (0.59 mg/L), the concentration in the solution decreases during the whole experimental duration (except cube I, 14 days, 90 °C and cube N, 14 days, 30 °C) down to 0.15 mg/L (30 °C) and 0.08 mg/L (90 °C) for ^{68}Zn and 1.14 mg/L (30 °C) and 0.13 mg/L (90 °C) for ^{67}Zn (Fig. 2 D, H).

3.2.5. Phosphorus

Phosphorus concentrations were measured only qualitatively using a Spectro Vision ICP-OES at the Institute of Geosciences, University of Mainz (Fig. S3). The absolute concentration values could not be established, because the analytical procedure was not validated for this high concentration of phosphorous, but the trend can be used, as the matrix of the samples did not change significantly and the reproducibility of the measurements was ensured. Phosphorous was absent in the initial tracer solution, but increased strongly after the first days of experiment. However, the P concentration then decreased over the progression of the remaining experiment, especially for the 90 °C experiment.

3.3. Element concentration profiles across dental cubes

Concentration of Ca, P, Mg, Zn, and Sr were measured using electron microprobe analysis. In both, enamel and dentin the concentrations do not show significant changes within the EPMA uncertainties of approximately 3 % (Weber et al., 2020b) during the 63 days of the 30 °C experiment (Fig. 3). Dental cubes placed in the 90 °C solutions show for the dentin slightly higher Ca (≈ 10 %) and P (≈14 %) concentrations after 21 days (Fig. 3). The Mg and Zn concentration of the inner dentin immersed for four days still shows an unreacted core area, while the outer ≈ 200 μm are clearly altered. After seven days of treatment, Mg and Zn in the dentin are altered throughout. While Zn concentration in dentin increases (up to 90 times above the range of natural variability), Mg decreases down to about 80% less Mg than the unaltered dental cube and the range of natural variability (Fig. 3). The enamel does not show significant changes during the 90 °C experiment (Fig. 3).

3.4. Isotope ratios of Mg, Ca, Zn and Sr across dental cubes

Isotope ratios were measured using the count rates conducted by LA-ICP-MS. Solutions bases Ca and Sr, as well as in-situ ^{87}Sr/^{86}Sr profiles were measured using (LA-)MC-ICP-MS. The untreated dental cube D was analysed as a reference material together with the treated samples to test the reproducibility of the measurements between different days of analysis. For the isotopes of interest, the mean values of the concentration of enamel and dentin lie within one standard deviation for all days of analysis (Table S5). Therefore, the LA-ICP-MS data of the different days of analysis are comparable among each other.

Solution based ^{87}Sr/^{86}Sr analyses of the unaltered enamel (AG-Lox) yielded an average value of 0.70999 ± 0.00003 (1SD, n = 6, MC-ICP-MS), in perfect agreement with LA-MC-ICP-MS results of 0.71003 ± 0.00009 (1SD, n = 23). Stable Sr ($\delta^{88/86}Sr_{NIST987}$) analysis of the unaltered enamel (AG-Lox) yield an average of −0.31 ± 0.05 ‰ (1SD, n = 5) and Ca isotope analyses yielded an average $\delta^{44}Ca_{NIST\text{-}SRM\ 915a}$ (^{44}Ca/^{42}Ca) of −0.56 ± 0.12 ‰ (1SD, n = 18). Both Sr and Ca isotope composition were measured using MC-ICP-MS.

The calculated isotope ratios of all four elements Mg, Ca, Zn and Sr in the dental tissues indicate that the dentin generally shows more pronounced alteration effects in comparison to the enamel during the experimental duration of the experiments for both temperatures (Figs. 4–6, Figs. S4–S13).

However, samples immersed at 30 °C in the tracer solution show only slight alteration effects in both enamel and dentin. Generally, the enamel shows only a narrow alteration rim of 25–50 μm for ^{44}Ca/^{42}Ca, ^{67}Zn/^{64}Zn and ^{87}Sr/^{86}Sr (Fig. 4, Fig. S4) in comparison to the dentin with an alteration rim of up to 150–200 μm from the outer tissue surface (Fig. 4). No correlation between the alteration depth and the duration of the experiment was detected. For ^{25}Mg/^{24}Mg, no distinct alteration is detectable in enamel (Fig. 4). However, a small decrease in all ^{n}Mg/Ca during the 30 °C experiment is visible for the outer 50–75 μm in the enamel (Fig. S5). Since all ^{n}Mg/Ca ratios decrease the same way, no change in the isotopic ratio occur. In addition, an increase of all ^{n}Zn/Ca ratios has been observed in the outer part of both enamel (up to 100 μm) and dentin (up to 150 μm), with the ^{67}Zn/Ca being at least one order of magnitude more enriched than the other ^{n}Zn/Ca ratios (Fig. S6 and S7). This is in accordance with the increase in ^{67}Zn/^{64}Zn shown in Fig. 4 and S8, as well as with the data of the tracer solution, which is reflecting a loss of ^{67}Zn from the solution. The enamel from the sample immersed for seven days (sample K), however, shows a different alteration pattern in the isotope ratio and the alteration depth, up to 100 μm in Ca, Sr and Zn and only a very minor (≈ 20–25 μm) alteration depth in Mg. This pattern is not visible in the dentin of sample K (Fig. 5). The dentin of samples treated up to 63 days at 30 °C show alteration rims up to 200 μm for ^{44}Ca/^{42}Ca, ^{67}Zn/^{64}Zn and ^{87}Sr/^{86}Sr. The ^{25}Mg/^{24}Mg shows an alteration

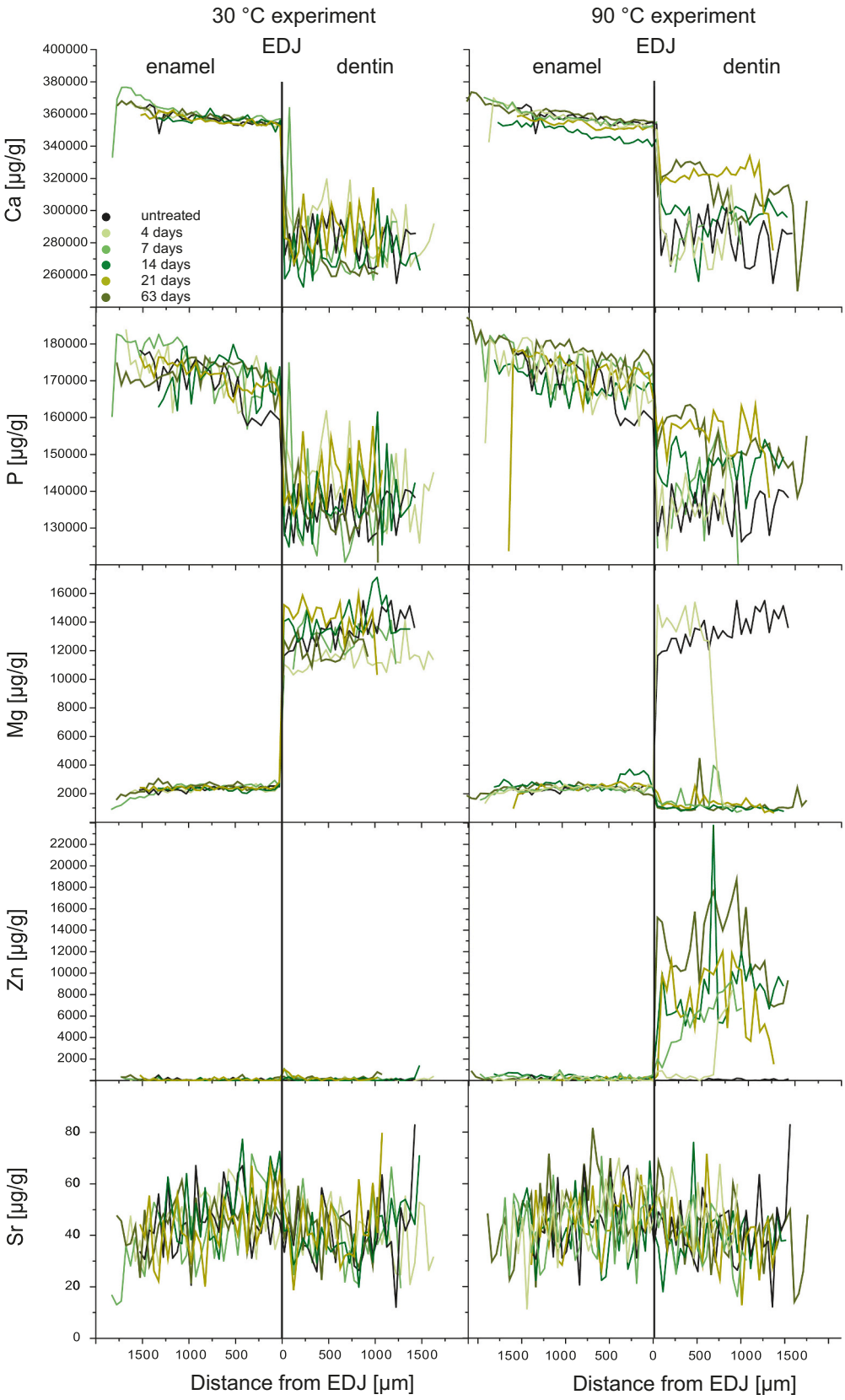

Fig. 3. Results from EMPA for the in-vitro experiment. Major and trace element concentration profiles of enamel and dentin across the enamel dentin junction (EDJ) determined by EMPA, lines are centred to the EDJ. Concentration profiles of dental cubes immersed for different reaction times of 4–63 days in to ^{25}Mg, ^{44}Ca, ^{67}Zn and ^{86}Sr enriched tracer solution are given for both reaction temperatures 30 °C and 90 °C.

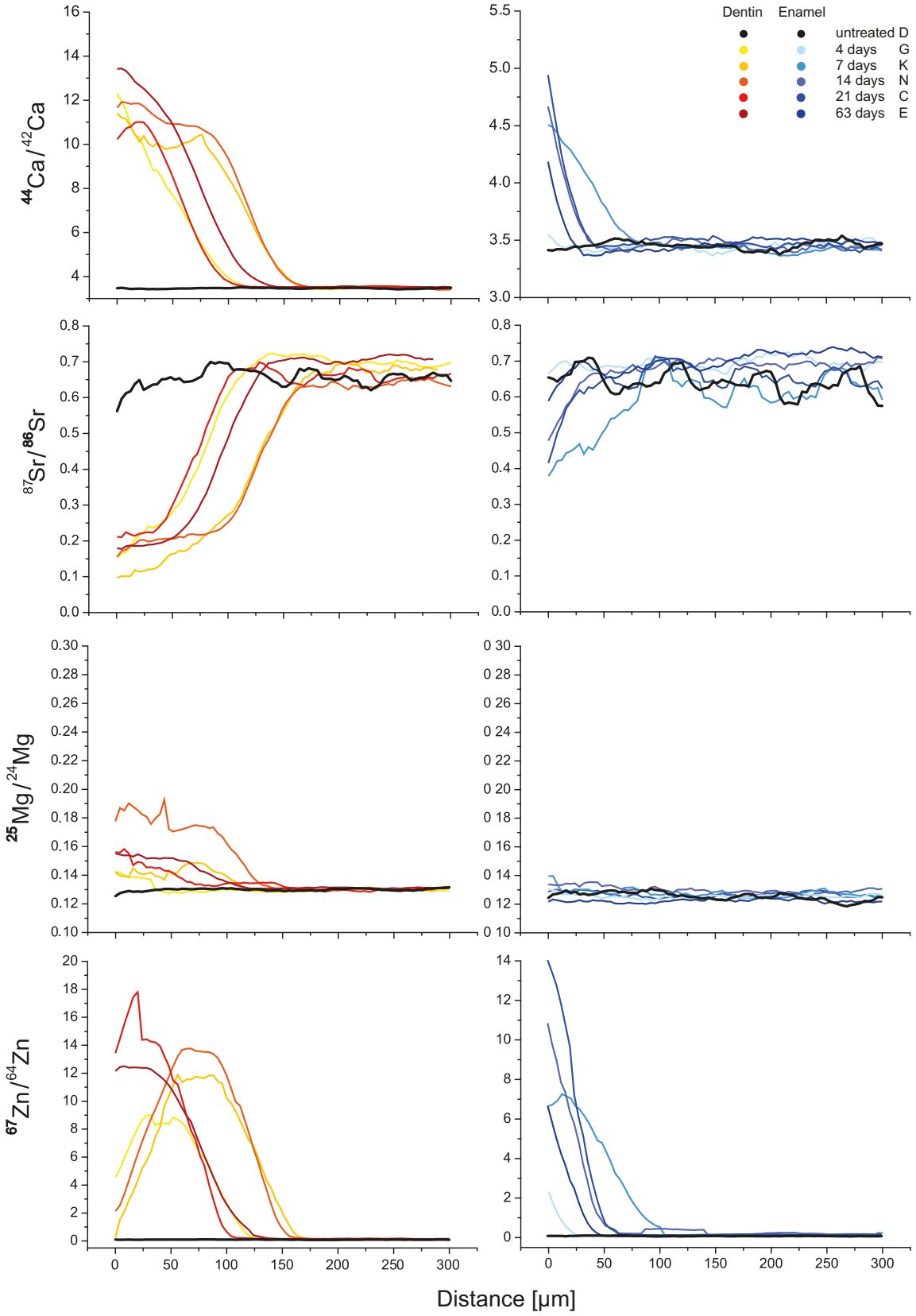

Fig. 4. Profiles of Ca, Mg, Sr and Zn isotope ratios measured in-situ by LA-ICP-MS from the outer cube boundary 300 µm into the dentin (left) and enamel (right) of experimentally altered dental cubes, respectively. The cubes were immersed in isotopically (^{44}Ca, ^{26}Mg, ^{86}Sr, ^{67}Zn) enriched tracer solution at 30 °C for increasing durations from 4 to 63 days.

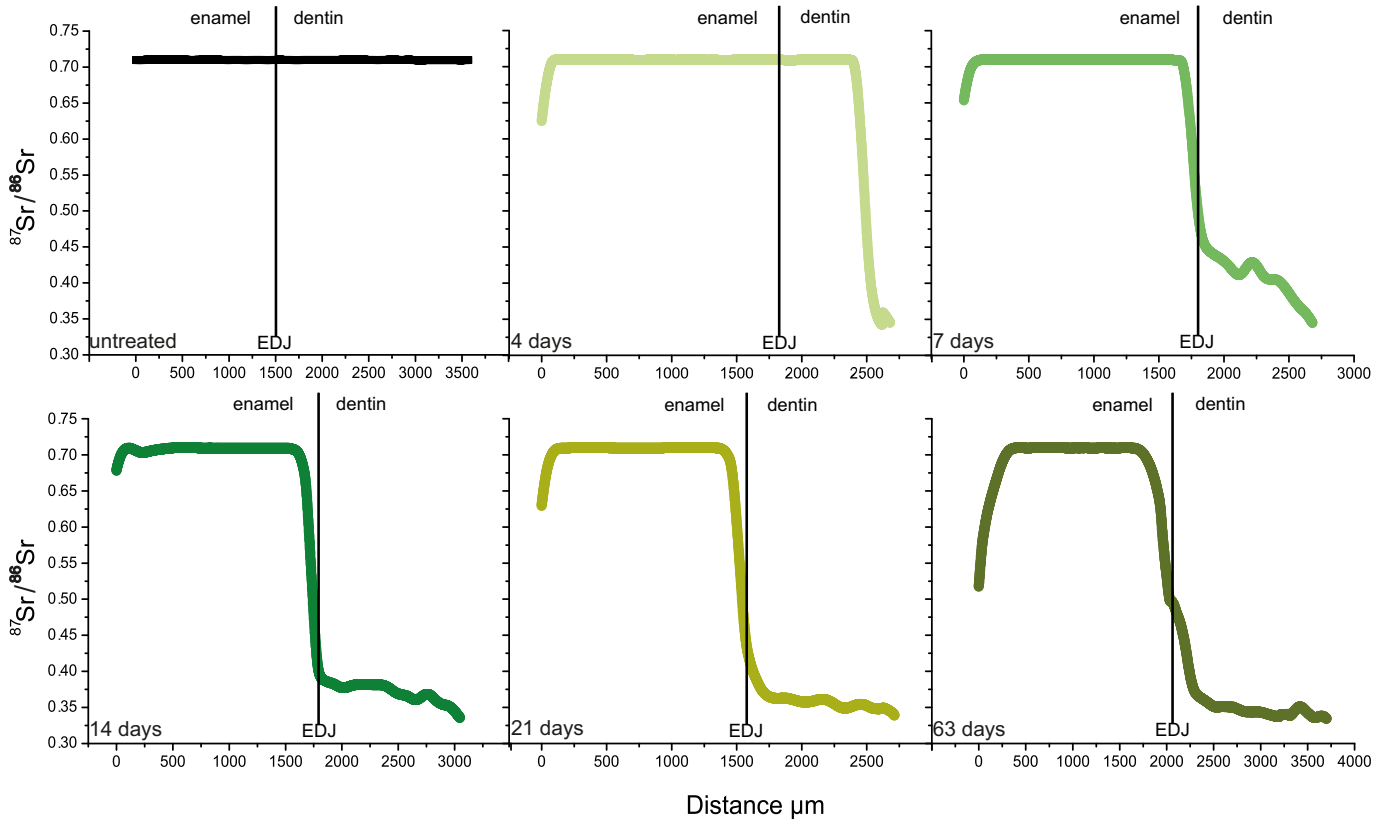

Fig. 5. The $^{87}Sr/^{86}Sr$ profiles measured in-situ by LA-MC-ICP-MS across experimentally altered dental cubes starting from the outer boundary of the enamel perpendicular across the enamel-dentin junction (EDJ). The unaltered sample (black bold line) is plotted in comparison to those from the 90 °C experiments of increasing durations from 4 to 63 days.

in the outer 150 µm, but not as pronounced as for the other three isotope ratios (Fig. 5). This agrees with the $^{n}Mg/Ca$ ratios for the outer dentin, which also show a decrease of $^{n}Mg/Ca$ for at least 150 µm. However, the $^{25}Mg/Ca$ is slightly elevated in comparison to the other $^{n}Mg/Ca$ ratios (Fig. S8), which is in line with the increase in $^{25}Mg/^{24}Mg$. The innermost part of all dental cubes treated with the solution at 30 °C does not show any sign of alteration of the enamel and dentin in the area around the EDJ.

The enamel of dental cubes immersed at 90 °C in tracer solution shows alteration rims in the outer part of the samples. The highest degree of alteration occurs in the experiment with the longest duration (cube F) for all isotope ratios, with alteration depths of up to 350 µm for $^{87}Sr/^{86}Sr$ (LA-MC-ICP-MS) (Fig. 5) and of ≈ 100 µm for $^{25}Mg/^{24}Mg$ and $^{67}Zn/^{64}Zn$, ≈ 150 µm for $^{44}Ca/^{42}Ca$ (Fig. 6) and. All other experiments of different, shorter durations show consistently an alteration rim of around 50–100 µm for Ca, Zn and Sr isotopes and almost no alteration of the $^{25}Mg/^{24}Mg$. In contrast, the $^{n}Mg/Ca$ is significantly lower than for the untreated sample (Fig. S9), while the $^{25}Mg/Ca$ is again higher compared to other $^{n}Mg/Ca$ ratios. No systematic increase of the alteration depth is visible with prolonged experimental duration.

Samples kept at 90 °C in the tracer solution show strong alteration effects, especially in the dentin. Only the sample with the shortest experimental duration (cube A, 4 days) still has an unaltered zone in the inner dentin and an alteration rim of ≈ 150 µm visible in the $^{44}Ca/^{42}Ca$, $^{87}Sr/^{86}Sr$, and $^{25}Mg/^{24}Mg$ (Fig. 6). Samples treated for a longer duration of a week or more do not have any unaltered dentin remaining (Fig. 5). Solution based Sr isotope analyses dentin from the altered dental cube H (7 days) yield a $^{87}Sr/^{86}Sr$ of 0.35680 ± 0.00001 (2SE, $n = 1$) and a $\delta^{88/86}Sr$ of −720.62 ± 0.03 ‰ (1SD, n = 1) showing the strong alteration of the dentin. Also, the $\delta^{44/42}Ca$ value of 2941.5 ± 1.4 ‰ (1SD, n = 1) is strongly altered. However, $^{67}Zn/^{64}Zn$ shows only a narrow alteration rim of 50 µm even for the shortest experimental duration (cube A, Fig. 6). For samples treated for seven and 14 days, a gradual increase of the $^{67}Zn/^{64}Zn$ towards the inner dentin until ≈ 250–300 µm is observed. Only the sample with the longest experimental duration (sample F, 63 days) shows fully altered dentin in $^{67}Zn/^{64}Zn$. This is in agreement with the $^{n}Zn/Ca$ ratios, which show an alteration rim for $^{67}Zn/Ca$ of 300 µm after 14 days (Fig. S10). Interestingly, the $^{n}Mg/Ca$ decreased in comparison to the initial ratio in all dentin cubes treated in the 90 °C experiment, indicating a Mg loss (Fig. S11). Nevertheless, the $^{25}Mg/Ca$ is higher than the two other $^{n}Mg/Ca$ ratios, confirming the increase in $^{25}Mg/^{24}Mg$ (Fig. 6). The LA-MC-ICP-MS $^{87}Sr/^{86}Sr$ clearly shows a fully altered dentin after seven days. At this point, the alteration starts to penetrate across the EDJ into the enamel, clearly visible in the longest duration experiment (cube F, Fig. 5). An interesting feature is visible for Sr in the $^{n}Sr/Ca$ ratios of the dentin (Fig. S12). While the $^{86}Sr/Ca$ is increasing in the treated samples, the $^{88}Sr/Ca$ ratio is slightly decreasing. This feature is especially pronounced in the dentin and only slightly occurring in the enamel (Fig. S13).

3.5. Changes in bioapatite mineralogy assessed by Raman spectroscopy

Raman spectroscopy was used to investigate potential modifications of the biogenic apatite in both dental tissues, enamel and dentin, of each sample (Figs. 7 and 8). Fig. 7 shows Raman spectra in the frequency range of 700–1450 cm^{-1} taken from the outer 120 µm of the dentin (Fig. 7A). A frequency range of 360–1200 cm^{-1} was chosen for spectra from the outer rim of the enamel (Fig. 7B). Reference spectra of untreated dentin and enamel as well as synthetic hydroxylapatite (HAp) are also included.

A comparison made of the reference spectra of both tissue types and the synthetic HAp (Fig. 7) reveal that the most intense feature is a band

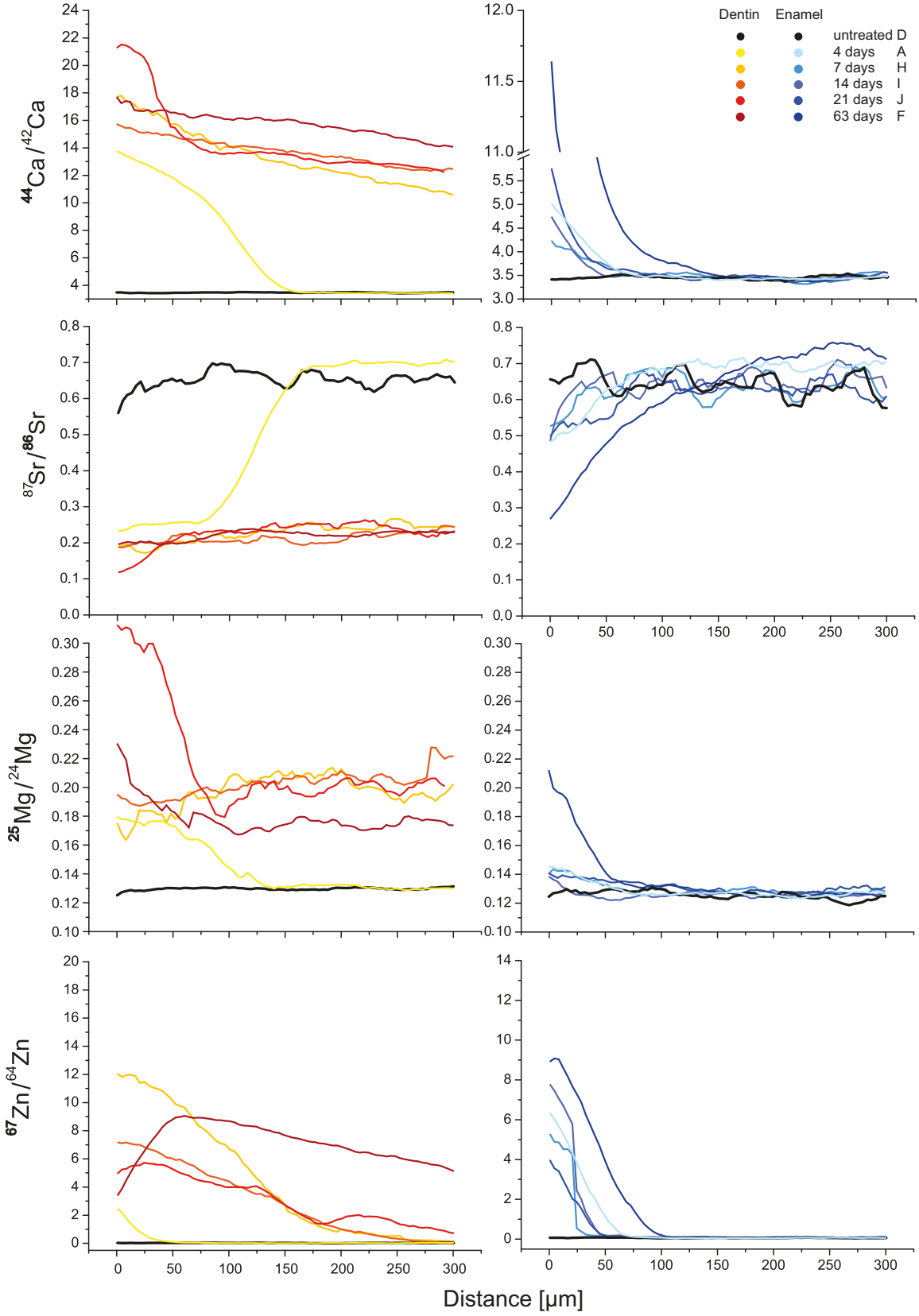

Fig. 6. Profiles of isotope ratios for Ca, Mg, Sr and Zn measured in-situ by LA-ICP-MS from the outer boundary of the cube 300 µm into the dentin (left) and enamel (right) for dental cubes of the in-vitro alteration experiments in isotopically (^{44}Ca, ^{26}Mg, ^{86}Sr, ^{67}Zn) enriched tracer solution at 90 °C for increasing durations from 4 to 63 days.

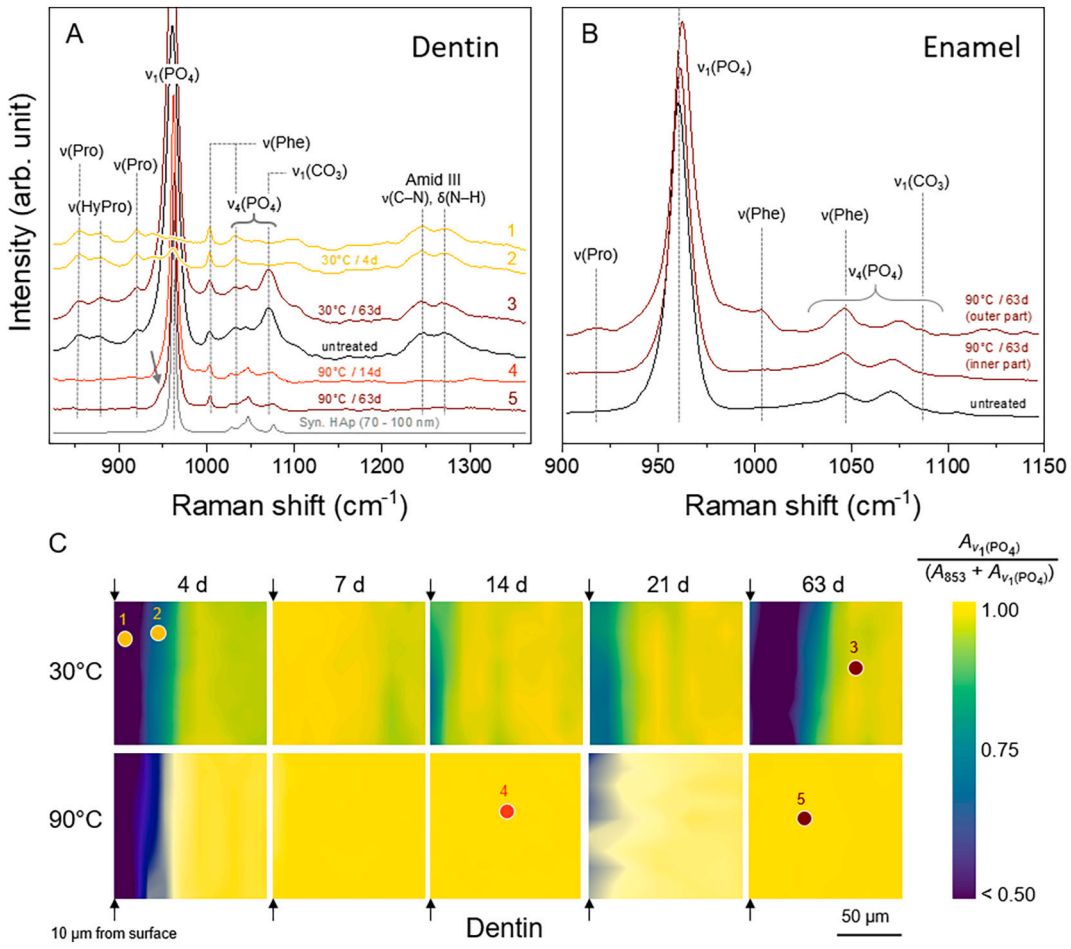

Fig. 7. Raman spectra of dentin A. and enamel B. for different experimental durations and temperatures. Spectra were normalized to the $v_1(PO_4)$ intensity. Grey arrow in A represents the narrowing of the $v_1(PO_4)$ band near 960 cm^{-1} by the appearance of a small shoulder near 948 cm^{-1}. Location of respective Raman spectra in the dentin are displayed as circle on the hyperspectral images shown in C. Each hyperspectral image represents an area of 120 × 120 µm. The colour coding shows the integrated intensity of the $v_1(PO_4)$ band relative to the proline band near 853 cm^{-1}.

at ~960 cm^{-1}, which is attributed to the fully symmetric stretching mode of phosphate ($v_1(PO_4^{3-})$). In HAp the shape of this band is symmetric, whereas in dentin and enamel spectra a slight asymmetry of the $v_1(PO_4^{3-})$ band can be observed on the lower frequency side, which is most likely caused by an underlying band at 950 cm^{-1} that has also been observed in other studies on bone apatite (Pasteris and Ding, 2009; Asjadi et al., 2019). Broad and less intense Raman bands between 1040 and 1090 cm^{-1} are attributed to the PO_4^{3-} antisymmetric stretching modes. However, the v_3 band near 1070 cm^{-1} overlaps with v_1 band of the carbonate unit near 1079 cm^{-1} ($v_1(CO_3^{2-})$). Dentin is further distinguished by a number of broad bands that are related to collagen vibrations: proline (853 and 917 cm^{-1}), hydroxyproline (873 cm^{-1}), phenylalanine (~1001 cm^{-1}) and amid III, consisting of v(C—N) and δ(N—H) modes (1243–3120 cm^{-1}).

The treatment in solutions at 30 °C and 90 °C affected the dental hard tissues differently, enamel experienced distinctly less modifications than dentin (Fig. 7). For dentin, representative spectra were selected from different locations on the sawed surface of the treated cubes for different reaction durations and at different temperatures (Fig. 7A). The exact locations of the spectra are displayed as circle on the hyperspectral images in Fig. 7C, where the colour of the respective circle corresponds to the colour of the spectrum. Each hyperspectral image covers an area of 120 × 120 µm with one collected spectrum each 10 µm. Spectra 1 and 2 were taken close to the rim of the dentin sample which was exposed for 4 days at 30 °C to the tracer solution. Here, the collagen bands are still detectable in the peripheral areas, whereas the initially most intense $v_1(PO_4)$ band is not detectable (spectrum 1) or shows only weak intensities (spectrum 2), in both spectra. The $v_1(CO_3)$ band is also no longer detectable . These spectral observations demonstrate that the inorganic component (i.e. bioapatite) of dentin dissolved, whereas the organic material was preserved.

Spectrum 3 was collected from the inner part of the 120 µm thick rim of a sample reacted for 63 days at 30 °C. This spectrum is comparable to those of the untreated sample, suggesting that no significant alteration occurred. In the hyperspectral image shown in Fig. 6C, however, it is clear that within the outermost 50 µm, the dentin has been strongly altered, i.e., this area is characterised by a low intensity ratio between the v_1 phosphate and the collagen bands. Spectra 4 and 5 were taken from dentin samples reacted at 90 °C for 14 and 63 days, respectively, and were taken from the inner part of the mapped area. The most prominent feature is again the $v_1(PO_4)$ band near 960 cm^{-1}, which, however, became sharper and blue shifted with increasing reaction time. The narrowing of this band is evident in spectrum 5 by the appearance of a small shoulder near 948 cm^{-1} (grey arrow in Fig. 7A). This band is also present in spectra from synthetic HAp, but has not yet been convincingly assigned. However, this could possibly reflect the splitting of the $v_1(PO_4)$ vibration of the free tetrahedron by the crystal field (Asjadi et al., 2019). It is usually hidden below the $v_1(PO_4)$ band (Pasteris and Ding, 2009), which was accounted for in this study by using an asymmetric Gauss-Lorenz function to fit the overall profile of this band. Moreover, both spectra no longer exhibit the broad $v_1(CO_3)$ band near 1070 cm^{-1}, suggesting the loss of carbonate from the dentine bioapatite phase and

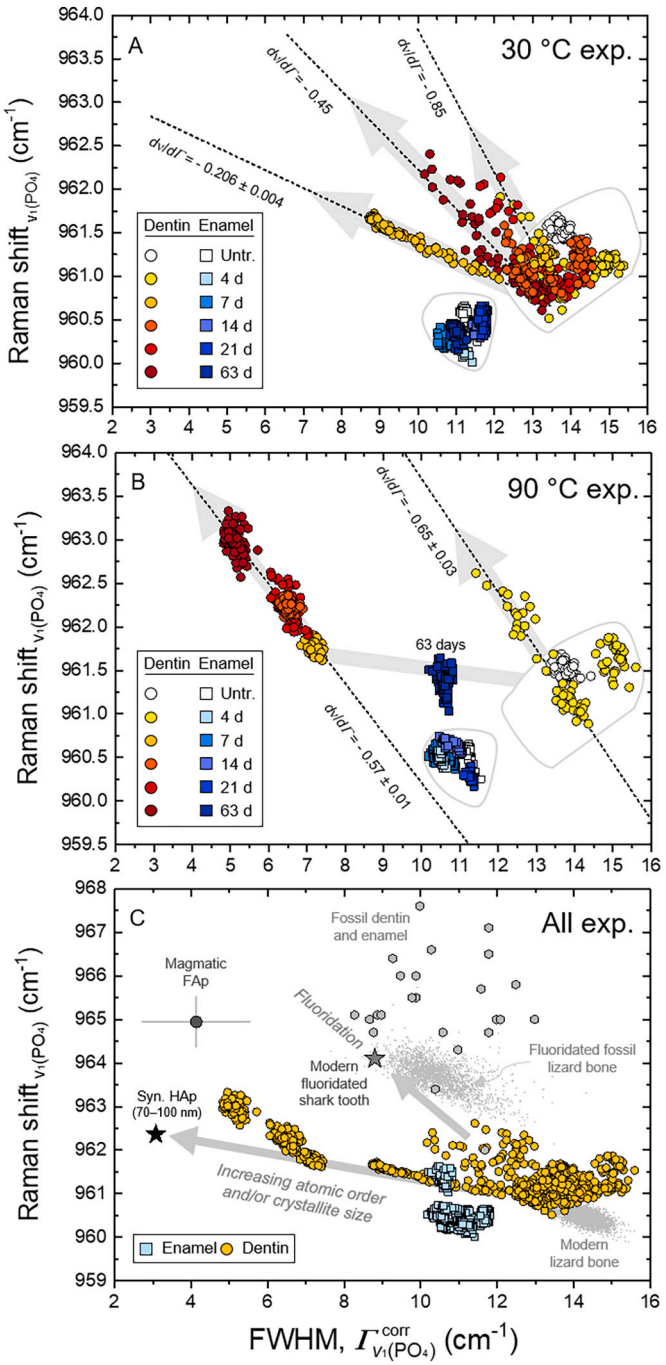

Fig. 8. The Raman shift of the $v_1(PO_4)$ band as a function of its width (corrected FWHM, $\Gamma^{corr}_{v1(PO4)}$) for dentin (yellow to red colours) and enamel (blue colours). A. Data from the 30 °C experiment, B. from the 90 °C experiment, and C. from both experiments in comparison with data from different modern and fossil bones (Pasteris and Ding, 2009; Barthel et al., 2020) and teeth (Thomas et al., 2007), as well as from synthetic HAp (Asjadi et al., 2019) and magmatic FAp (own, unpubl. data). Arrows mark distinct trends that show different slopes of $d\nu/d\Gamma$ in (A) and (B) enclose the field for untreated and unaltered dentin and enamel, respectively. (For interpretation of the references to colour in this figure legend, the reader is referred to the web version of this article.)

thus complete reorganisation of its apatite crystal lattice. It is also noteworthy that the ν(C—C) vibration of the aromatic phenylalanine ring near 1001 cm^{-1} is clearly detectable but this is the only significant remaining collagen-related Raman signal.

The only significant visible spectral changes in enamel were observed on the rim of the enamel sample treated at 90 °C for the longest reaction duration (Fig. 7B). The spectra from the outer part of this sample have a distinctly blue shifted $v_1(PO_4)$ band compared to the spectra of the inner part and the untreated enamel reference. Furthermore, two weak bands at 917 cm^{-1} (proline) and 1001 cm^{-1} (phenylalanine) as well as weak amid III bands, all assigned to collagen vibrations, are significantly more intense than in the spectra from the inner part of the enamel and the untreated enamel reference.

In order to quantify potential modifications within the bioapatite lattice, the position and width of the $v_1(PO_4)$ band were determined by least-squares fitting of an asymmetric Gauss-Lorentz function and plotted against each other in Fig. 8. Raman data from fossil dentin and enamel, modern and fluoridated fossil lizard bone, modern fluoridated shark tooth, magmatic fluorapatite (FAp), as well as synthetic HAp are plotted as references in Fig. 8C.

As already observed in the Raman spectra, enamel is distinctly less reactive than dentin. Especially, the Raman spectra from the enamel samples reacted at 30 °C for different durations (Fig. 8A, blue symbols) do not reveal any significant changes, as the samples, irrespective of the experimental duration, all plot in the same area. Any difference merely reflects the natural variability of the starting material. Similarly, samples treated at 90 °C for up to 21 days do not show any significant changes (Fig. 8B). However, after an experimental duration of 63 days, the $v_1(PO_4)$ band position increased significantly by about 1 cm^{-1}, whereas the bandwidth did not change significantly. This frequency shift is also directly visible in the Raman spectrum shown in Fig. 7B.

Under the microscope differently pronounced but clear reaction rims are visible in the dentin part of all samples treated at 30 °C (Fig. S14). However, there is no clear correlation between the width of the reaction rim and the duration of the experiment, as also deducible from Fig. 7C. In any case, all samples from the 30 °C experiments have preserved an apparently unreacted zone within the measured areas (Fig. 7C). Data points from this zone cluster in the diagram frequency versus width of the $v_1(PO_4)$ band between about 960.5 and 961.7 cm^{-1} and between 12.0 and 15.5 cm^{-1}, respectively (marked area in Fig. 8A and B). These ranges essentially represent the natural, spectral variability of the starting dentin material. In the measured outer part of the treated dentin samples, substantial band parameter changes occurred with increasing reaction time both at 30 °C and 90 °C (Fig. 8A and B). At 90 °C and reaction times larger than 7 days, the measured area has completely been altered, particularly recognisable by a significant reduction of the bandwidth (Fig. 8B), whereas for samples treated at 90 °C for 4 days, only the data pattern is still comparable to that observed for the 30 °C experiments (Fig. 8A).

The overall pattern is complex and cannot be explained by a single process. Whereas in a perfect crystalline solid the long-range order of the lattice makes the correlation length of the normal-mode vibration infinite, limiting Raman scattering to zone-centre (q = 0) optical phonon modes, in defect-rich or nano-crystalline materials, such as dentin apatite, the relaxation of the momentum selection rule allows a greater range of vibrational modes to contribute to Raman scattering. This results in a redshift of the phonon frequency and a decrease in the phonon lifetimes, i.e., a broadening of Raman bands. In the anharmonic approximation, the phonon frequency (real part) and the phonon lifetime (imaginary part) should be linearly related to each other via Kramers-Kronig relationship. Indeed, we observe different, nearly linear data arrays in the data set of dentin treated at 30 °C that are characterised by different slopes $d\nu/d\Gamma$, ranging from -0.206 ± 0.004 to about -0.85 (Fig. 8A and B). In particular, the dentin altered for 7 days at 30 °C shows an evolution of Raman spectral parameters towards synthetic hydroxylapatite (crystallite sizes between 70 and 100 nm) with a slope $d\nu/d\Gamma$ of -0.206 ± 0.004, whereas all other experiments resulted in steeper trends that point them towards fluoridated fossil tooth and bone references as shown in Fig. 8C. We also note that after 7 days at 90 °C, the dentin band parameters plot at the trend towards synthetic HAp, but for longer durations the slope $d\nu/d\Gamma$ again became steeper, i.e., $d\nu/d\Gamma = -0.57 \pm 0.01$, indicating a change in the recrystallisation

process towards FAp, due to higher wavenumbers.

4. Discussion

4.1. Weight loss and mass balance

The weight loss observed in samples immersed in acidic (≈ pH 1) tracer solutions at 30 °C and 90 °C is the result of material loss by dissolution of dental material (preferentially bioapatite), as indicated by increasing Ca and P content in the remnant solution (Table S2, Figs. 2 and 3). This dissolution of bioapatite caused an increase of solution pH from 1 to about 6–7. The degree of alteration observed at 30 °C and 90 °C seem to be different for the elements of interest. While both Ca and Sr concentrations show a similar temporal evolution in the tracer solution, both at 30 °C and 90 °C, Mg and especially Zn seem to be controlled by different reaction mechanisms. This becomes evident by the differences in material loss of the dental cubes between both experimental temperatures and by comparing those data with the changes in solution composition over time. Based on the observed concentrations of the doped and undoped isotopes of interest in the solution, it is possible to calculate the expected material loss of the dental cubes by calculating a mass balance based on the solution concentrations (Table S6). However, this approach is limited by some assumptions, i.e. (a) the natural variability in element concentrations across the dental cubes, resulting in uncertainties of the average concentration of the dissolved material, (b) the uneven surface of the dental cubes, which can cause an enhanced dissolution of one cube in comparison to the other, due to differences in surface area, (c) the concentration difference of the isotope/element of interest in the initial solution and in the solutions from different time intervals of the immersion experiment. The latter is especially crucial for ^{44}Ca, which has already a high concentration in the raw solution and does not increase as much as the ^{43}Ca, i.e. resulting in a high background concentration in the starting solution. These limitations might also explain the non-linear behaviour of the material loss with increasing time. Another explanation for the non-linear behaviour could also be the decreasing driving force of the reaction caused by the increasing pH value. However, there are as well several points affecting the accuracy in weighing, i.e. varying water content in the dental cube. Based on the results from the solution (Fig. 2), we calculated the absolute amount of each isotope (^{25}Mg, ^{26}Mg, ^{43}Ca, ^{44}Ca, ^{67}Zn, ^{68}Zn, ^{86}Sr, ^{88}Sr), based on their concentration, the known volume of each solution (2 mL, see "Materials and Methods, Tracer solution"), the natural abundance of each isotope (Meija et al., 2016), the elemental concentrations of the unaltered dental cube (Table S5) and the weight of each dental cube (Table 1). Calculations for Zn have not been performed, since the Zn concentration in the solution is decreasing with time, i.e., there is no Zn dissolution from the dental cube. The same trend was observed for the calculations using ^{44}Ca and ^{86}Sr during the 90 °C experiment. Therefore, these calculations have also been excluded from the Fig. 9. For the 30 °C experiment, the calculations based on ^{43}Ca, ^{88}Sr, ^{25}Mg and ^{26}Mg show the best agreement with the measured weight loss, while ^{44}Ca and ^{86}Sr seem to underestimate the dissolved apatite material. During the 90 °C experiment, both Mg concentration calculations, as well as the calculation based on ^{43}Ca, overestimate the weight loss. The best agreement was found between the measured weight loss and the mass balance model based on the ^{88}Sr. This is especially interesting, since we observe a decrease of the ^{88}Sr/Ca in the dental cubes in the 90 °C experiment (Fig. S12 and S13). This evolution indicates, that ^{88}Sr seems to most accurately reflect the bioapatite dissolution process of the dental cubes during this experiment. In contrast, ^{44}Ca and ^{86}Sr show a decreasing trend in the solution data and are most likely involved in an opposing trend and increase due to mineral re-precipitation along the dental surface (Fig. S15C).

4.2. Evolution of the tracer solution and dental cubes

The composition of the tracer solution evolves differently for the elements enriched therein, but also for different isotopes of the element of interest at 30 °C and 90 °C (Fig. 2), whereby slight positive shifts in the mass fraction might be due to some evaporation loss of the tracer solution during the experiment, especially during the 90 °C experiment. For Mg, a clear increase for both isotopes ^{25}Mg (doped) and ^{26}Mg (undoped) in the solution is observed at both temperatures. Interestingly, the increase in ^{25}Mg (~4.6 mg/L for 30 °C and ~ 9.1 mg/L for 90 °C) and ^{26}Mg (~4.8 mg/L for 30 °C and ~ 9.3 mg/L for 90 °C) reflects the natural isotopic composition of Mg (^{25}Mg ~ 10 % and ^{26}Mg ~ 11 %), suggesting that Mg is leached from the dental cubes. In general, during the 90 °C experiment the Mg concentration in the solution increased more than during the 30 °C experiment, indicating a higher dissolution of the dental material (Fig. S2). This agrees with the weight loss data of the dental cubes at 90 °C and 30 °C displaying a higher loss of 23.5 ± 2.3 % compared to 15.5 ± 1.5 %, respectively (Table 1). Magnesium is further dissolved with increasing duration of the experiment, which is in agreement with the decreasing ^{n}Mg/Ca in the dental cubes. All ^{n}Mg/Ca

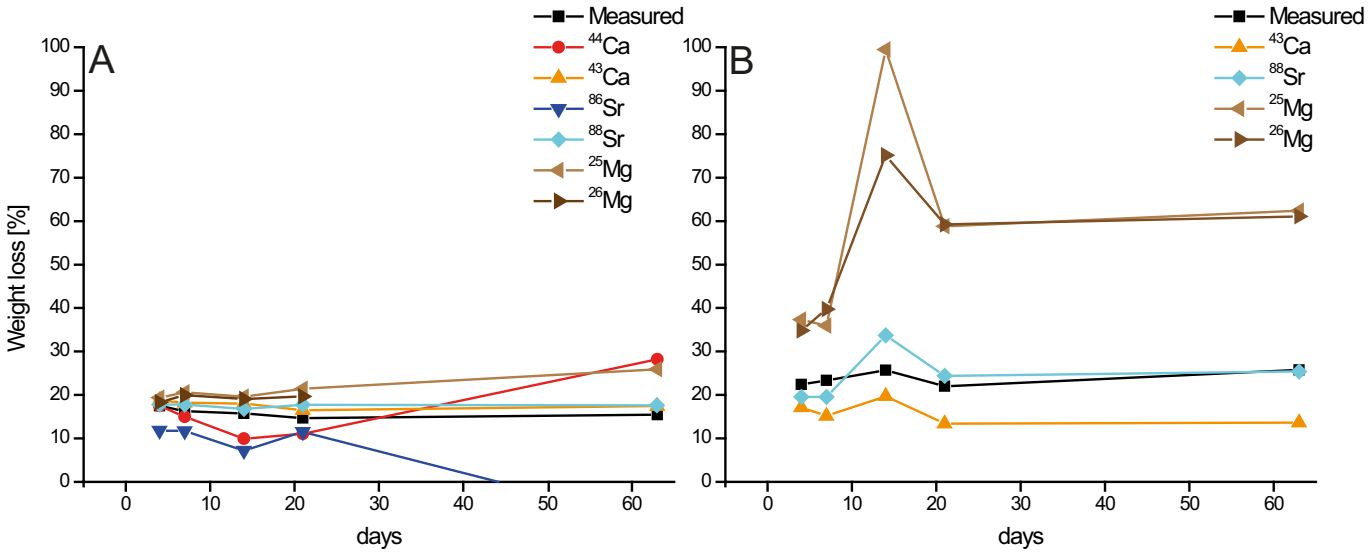

Fig. 9. Weight loss of the dental cubes based on the mass balance model for the A. 30 °C experiment and the B. 90 °C experiment. Note that in (B), the calculations based on ^{44}Ca and ^{86}Sr are not shown due to negative values (see text for details).

ratios decrease in altered dental tissue compared to the starting values of each dental cube before the experiment, especially in the dentin, which is completely overprinted in the 90 °C experiment and lost about 80 % of its Mg content (Fig. S8). However, the doped ^{25}Mg shows the highest ^{n}Mg/Ca ratio, both in the dentin and enamel after the 90 °C experiment. Since both, the lighter ^{24}Mg and the heavier ^{26}Mg are less concentrated in comparison to the ^{25}Mg with intermediate weight, no clear trend towards a preferential dissolution of heavier/lighter isotopes is detectable. This implies that the dissolution process out of the dental cube for the Mg is (mainly) controlled by the concentration gradient between solid dental material and the tracer solution, the latter being highly enriched in ^{25}Mg.

Zinc shows a completely different alteration behaviour, both in the solution and in the dental tissues, from Ca, Sr and Mg. Apart from two outliers for the 14 days experiment (Fig. 2), the Zn concentration in the solution shows an exponential decrease for the whole experimental duration under both temperatures (Fig. S.16). In addition, all ^{n}Zn/Ca ratios increase in the outer parts of the dental cubes, both for enamel and dentin (Fig. S6, S7 and S10). However, the ^{67}Zn/Ca increases the most, leading to an increased ^{67}Zn/^{64}Zn (Fig. 4, S5, S7). This implies that Zn is absorbed from the solution and incorporated into the apatite crystal lattice. If any Zn dissolution from the dental material occurs, this amount is several orders of magnitude lower than that of the Zn precipitation, i.e. there is a net accumulation of Zn in the outer rim of the dental tissues, both dentin and enamel. However, it is impossible to evaluate the amount of Zn dissolved in comparison to Zn incorporated. It is assumed that Zn is taken up into the dental material, substituting for the leached out divalent cations, such as Ca^{2+}, Mg^{2+} and Sr^{2+} in the crystal lattice of the apatite. Zinc distribution patterns comparable to our experiment have also been postulated for fossil aurochs bone fragments from the Neolithic (Reiche et al., 2003). The increase in ^{n}Zn/Ca ratios in the outermost parts of the dentin and enamel could be caused by incorporation of Zn from the tracer solution into the dental tissue or the possibility of contamination of Zn from either laboratory gloves during the handling of the samples (Garçon et al., 2017), or from the resin Technovit 5071 in which the samples have been embedded. An incorporation from the tracer solution, however, seems to be more likely, since there is no increase in ^{n}Zn/Ca ratios in the untreated cube, which were handled similar to the treated cubes. This is in good agreement with a recent Zn isotope study on human teeth that found no significant Zn contamination of enamel from gloves during tooth handling (Jaouen et al., 2020).

The evolution of Sr and Ca isotopes is similar during the experimental duration and the two temperatures, as expected from their similar chemical properties. However, the concentration changes of Ca in the tracer solution are even more pronounced during the 90 °C experiment. The ^{43}Ca and ^{88}Sr, which were not enriched in the tracer solution, both increase rapidly after the experiment started and almost stay constant during the full experimental duration (Fig. 2). Only for the 90 °C experiment, ^{43}Ca might show a slight decrease with increasing experimental duration (Fig. 2B). This indicates that Sr and Ca are both dissolved from the dental material into the solution. This dissolution is mostly happening during the first four days of the experiment and is significantly reduced afterwards. Due to buffering of the tracer solution by bioapatite dissolution, the pH increases up to 6 to 7 and the solution is no longer acidic. This prevents any significant further dissolution, since hydroxylapatite dissolution is highly dependent on pH and almost not soluble in neutral aqueous solutions (Fassbender et al., 1966; Berna et al., 2004).

For the doped ^{44}Ca and ^{86}Sr in the 30 °C experiment, also the solution concentration varies only slightly after initial dissolution within the first four days. However, for the 90 °C experiment, the doped isotopes of ^{44}Ca and ^{86}Sr decrease significantly in the tracer solution. Since there is no other sink (no precipitates that formed in the Teflon beaker) for the Ca and Sr than the dental cubes, the only explanation is that both are incorporated into the dental material, i.e. by re-precipitation as newly formed (synthetic) hydroxlyapatite (Fig. 8). The re-precipitation is only visible during the 90 °C experiment and therefore seems to be controlled mainly by temperature, i.e. a specific thermal activation energy is needed to induce the re-precipitation. Especially for supersaturated solutions, an equilibrium state can only be achieved when long experimental durations and/or highly elevated temperatures are used (Chander and Fuerstenau, 1984).

The differences in the concentration for the specific time intervals (i.e., 14 days at the 90 °C experiment) are again most likely due to the natural variance in the trace element composition of the dental material between the different individual cubes. The imperfections of the crystal structure of bioapatite can therefore favour the mineral dissolution (Mayer and Featherstone, 2000). As soon as hydroxylapatite starts to re-precipitate from the solution, the rate of precipitation is not only controlled by the availability of Ca^{2+} and PO_4^{3-} ions, but also by the surface of the dental cubes (Inskeep and Silvertooth, 1988). The surface area, as well as the inner enamel and dentin differs between the different dental cubes (Fig. S15).

In the 90 °C experiment, the doped isotopes (^{44}Ca, ^{86}Sr, ^{25}Mg) of the respective elements show a different evolution. There is no clear trend regarding the preferential precipitation of a lighter/heavier isotope. For Ca, the heavier ^{44}Ca is preferentially removed from the solution into the newly precipitated mineral, while for Sr, the lighter ^{86}Sr is preferentially incorporated. For the 90 °C experiment, the ^{88}Sr/Ca decreases over the duration of the experiment, while the ^{86}Sr/Ca increases. This trend is especially visible in the dentin, but also slightly visible for the outer enamel (Figs. S12, S13). This would imply a preferential incorporation of the lighter ^{86}Sr in comparison to the heavier ^{88}Sr. While this trend is known for fractionation along trophic food chains (Knudson et al., 2010), i.e. due to biological processes, the experimental setup is entirely inorganic and therefore should not favour the lighter isotope. Stable isotope fractionation in biological processes is typically in the permil or sub-permil range. In our in-vitro experiment probably no stable isotope fractionation might be visible for the precipitation of Sr (for Ca and Mg as well) from the tracer solution to the solid dental material, because the difference in the ^{86}Sr/Ca ratio is dominated by the excess of ^{86}Sr in the solution. We observe a preferred incorporation of isotopes with higher concentrations in the enriched tracer solution, rather than dependent on the isotopic weight. This is true for Ca (^{44}Ca is preferentially incorporated versus ^{43}Ca), Sr (^{86}Sr is preferentially incorporated versus ^{88}Sr), but also for Mg, where the intermediate, but more concentrated ^{25}Mg in preferentially incorporated in contrast to the lighter ^{24}Mg or the heavier ^{26}Mg (Figs. S9, S11). Since all three elements belong to the same group of earth alkaline elements they should react in a similar way in natural processes. Since there is no, or at least detectable isotope fractionation observed in these alteration experiments, it seems more plausible, that the re-precipitation process at higher temperatures is induced due to the oversaturation in the solution of solved calcium phosphate and the unproportionally higher abundance of the enriched ^{25}Mg, ^{44}Ca and ^{86}Sr in the solution, compared to ^{24}Mg, ^{26}Mg, ^{43}Ca and ^{88}Sr, respectively.

4.3. Implications for sampling of dental tissues for isotope or trace element analysis

Based on the laser ablation profiles isotope ratios of all four different isotope systems Ca, Sr, Mg and Zn display alteration rims of enriched concentrations in the outer enamel of at least ≈ 100 μm for both temperatures. For the lower temperature experiment (30 °C) no systematic extension of the alteration rim (i.e. penetration depth of the reaction zone) with increasing experiment duration was observed. Since the dental cubes are biological materials, natural variation in chemical composition and structural properties is likely. Therefore, deeper penetration depth of the alteration rim in single samples could be explained with a crack (Fig. S15B) or more porous enamel, which might function as a fluid pathway for the isotopic tracer solution deeper into the dental material. In the higher temperature experiment (90 °C), the

deepest reaction depth of around 150 μm was observed in the longest lasting experiment (cube F, 63 days). For all other experimental durations, no systematic increase could be detected, implying that a significant difference in alteration depth of the enamel only occurs at higher temperatures and long experimental durations. It could also be concluded that the main alteration processes took place during the first few days of experiment, while the pH value was only 1. As soon as the pH increases, the dissolution process likely stopped. In-situ LA-MC-ICP-MS $^{87}Sr/^{86}Sr$ analysis allows for a more sensitive and higher spatially resolved assessment of diagenetic alteration than LA-ICP-MS analysis. Therefore, the higher spatially resolved LA-MC-ICP-MS $^{87}Sr/^{86}Sr$ data shows, independent of experiment duration, an enamel alteration rim of 300 μm at 30 °C (Fig. S4) and up to 500 μm at 90 °C. Therefore, for sampling of fossil teeth for isotope analysis the removal of the outer few 100 μm of enamel is recommended to ensure the analysis of the least altered central part of the enamel. This may be feasible for mammal teeth with thick enamel, but may be problematic and not feasible for reptilian teeth with thin enamel, as well as for small-sized teeth. However, as the innermost enamel, along the EDJ, is also altered due to a penetration of the tracer fluid through the whole dentin and across the EDJ into the innermost few 100 μm of enamel (Fig. 5), this zone should ideally also be avoided for geochemical analysis assessing in-vivo compositions. The innermost, pristine zone in the central part of the enamel is shrinking from both sides with the duration of the alteration experiments (Fig. 5). After 63 days at 90 °C, there remains only a zone of ≈ 1 mm unaltered enamel, which is about ≈ 56% of the original enamel thickness of ≈ 1.8 mm. In contrast, dentin is much more prone to alteration than the enamel. Especially during the higher temperature experiment, a complete alteration of the ≈ 1.4 mm thick dentin is observed for all doped isotopes (^{25}Mg, ^{44}Ca, ^{67}Zn and ^{86}Sr) already after 7 days. This is probably caused by the lower apatite crystallinity, higher porosity, lower degree of mineralisation and higher content of organic matter (i.e. collagen) in the dentin compared to the enamel, making it much more prone to post-mortem alteration.

4.4. Dissolution and precipitation processes

The Raman spectra of enamel and the extracted spectral parameters, bandwidth and position, of the $v_1(PO_4)$ band display a higher resistance of enamel against alteration, matching with the expected higher apatite crystallinity of enamel compared to dentin. Due to the high crystallinity, the enamel is less vulnerable to changes during the lower temperature experiment (30 °C), where no changes in the Raman spectral parameters in the outer 120 μm were observed. Even at higher temperatures (90 °C experiment), only the enamel in the sample with longest exposure to the tracer solution show an increase of the $v_1(PO_4)$ band position in the outer 120 μm (Figs. 7 and S16). Note that band position is determined from the average P—O bond length involved in the symmetric stretching of phosphate (i.e. Popović et al., 2005). The higher band positions indicate a shorter P—O bond length, which could be caused by the incorporation of light ions from the doped isotope tracer solution on the Ca crystal lattice position. Fluorine is known to substitute on the OH-position in the apatite lattice and can cause also such a shift of the $v_1(PO_4)$ band to higher wavenumbers (Thomas et al., 2011). However, the tracer solution initially did not contain any F, therefore, in this special experimental setup, the only possible source of F are the reaction beakers consisting of Teflon, which is a synthetic fluoropolymer of tetrafluoroethylene. Especially for experiments with long durations at sub-boiling temperatures and initially low pH values, dissolution of F from the Teflon beakers seems plausible. This is further supported by the fact that a notable shift only occurred in the enamel experiment that ran for 63 days at 90 °C. The different $d\nu/d\Gamma$ trends are potentially a result of different F concentrations dissolved from the Teflon beakers, expect for the $d\nu/d\Gamma$ trends going towards synthetic HAp (Fig. 8C).

Modifications of the dentin Raman spectra and of the $v_1(PO_4)$ band confirm that dentin is much less resistant against alteration compared to enamel. Furthermore, the alteration processes of dentin samples progress continuously and are temperature-dependent. The reaction time seems to have only little influence at low temperatures, however temperaturehas a clear affect on dissolution of hydroxylapatite and a preservation of organic material. That the partial dissolution of the apatite component in the outer part of the samples relatively increased the proportion of collagen to bioapatite, as is also observed for the dentin samples, even at lower temperatures. Raman spectra of the dental cubes from the 30 °C experimental series display the dissolution of apatite in the outer dentin area exposed to the solution already after 4 days, while collagen is predominantly still preserved, indicating a preferred preservation of organic matter in this specific acidic environment at low temperatures (Fig. 7). In the 90 °C experimental series, the outer 120 μm of dentin were also completely altered already after 4 days. At higher temperature, degradation of the organic matter can be observed, while the bioapatite component remains preserved, even after long experimental durations. This is reflected by a strong shift of the $v_1(PO_4)$ band towards higher wavenumbers in samples with longer reaction duration at 90 °C (Fig. 8B), which hints towards a dissolution-recrystallisation process. From unaltered dentin Raman shift and FWHM display two different trends, one towards values of high bandwidth and slightly increasing band position and the other displaying increasing band position accompanied by a strongly decreasing bandwidth, reaching minimum values close to synthetic HAp (Fig. 8C).

A dissolution-recrystallisation process of the bioapatite would lead to higher apatite crystallinity, resulting in such an increasing $v_1(PO_4)$ band position and decreasing bandwidth. During the dissolution and recrystallisation of the apatite F and Zn got incorporated. Zinc is known (independent of Zn concentration) to reduce the reactivity of the dental material versus acids, causing less dissolution of the dental cubes after the initial experimental phase, as well as the formation of new and larger crystals (Featherstone and Nelson, 1980) with less structural defects (Nelson et al., 1982; Mayer and Featherstone, 2000). This would lead to the observed increased crystallinity and the decreased bandwidth in the Raman spectra. Furthermore, the lower Mg/Ca in the newly precipitated hydroxylapatite could also cause a higher crystallinity (LeGeros et al., 1996). Since Mg is leached out of the dentin, Sr and/or Zn seems most likely to substitute for Ca instead of Mg, causing the increase of the band position, when comparing Raman spectra with the laser ablation results.

The dissolution behaviour of Ca-apatites in acids, such as hydroxylapatite in HNO_3, can be described by different models and is still a matter of debate (see Dorozhkin, 2012 and references therein for a literature review of different models). However, such models are only of limited use to explain dissolution and precipitation of the bioapatite of the dental cubes used in this study. Furthermore, these models are not valid for experimental conditions with pH < 2 and temperatures above 70 °C (Dorozhkin, 2012). Since isotopic fractionation seems to be only of minor importance for the processes observed in the experiment, we mainly use concentration differences and diffusion effects on the solid/liquid interface as explanation. As soon as the solid material (i.e. the dental cube) gets in contact with the tracer solution, a small layer of solid/liquid interface develops (DePaolo, 2011). This induces the chemical interaction of the solution with the apatite (Pearce, 1988), and the exchange of ions from both reservoirs within the solid/liquid interface. The components of the solution will absorb onto the surface of the dental cubes and induce a chemical exchange of the surface layer, i.e. causing the crystal surface to lose some of its components, such as Ca^{2+}, Sr^{2+}, Mg^{2+} and PO_4^{3-}. Depending on the ionic diffusion gradient, ions from the bulk solution or the dental material are exchanged within this interface layer and ultimately either transported into the solution, or incorporated into recrystallised dental material (Dorozhkin, 2012). Therefore, the large concentration differences in the tracer solution between the different isotopes, ^{44}Ca vs. ^{43}Ca and ^{88}Sr vs. ^{86}Sr, will ultimately be responsible for the different isotope evolution, while the element concentration stays consistent during the 90 °C experiment.

Our experiments demonstrate that non-traditional isotopes such as

Ca, Sr, Zn and Mg increasingly used for dietary and physiological reconstructions are prone for diagenetic alteration in fossil teeth. Particularly when exposed to low pH conditions, as for example during digestions. Stomach acids of predators and scavenger have very low pH values (Beasley et al., 2015) and might aggressively attack dental surface already within short durations, as seen in the presented experiment. Especially dentin is vulnerable for alteration and should be avoided. But enamel, especially the outer and innermost few hundred micrometers, can also be altered when exposed to diagenetic fluids, depending on the time of burial and the physico-chemical conditions in the diagenetic setting as well as the tooth geometry. The dental cubes analysed in this study originate from a large mammal species, however, different species have potentially different degree of enamel mineralisation and microstructure (Berkovitz and Shellis, 2016, 2018). Chemical alteration of fossil dental material might differ among each other, the presented results might be most applicable on larger mammals with similar hydroxylapatite microstructure than reptiles, with generally thinner enamel layers and different microstructures. More experiments including different species are necessary to address the vulnerability of enamel from different species. The enamel along the EDJ can be affected by alteration of solutions penetrating into the enamel from the dentin. To obtain pristine, in-vivo isotope compositions it is thus important to carefully assess the chemical and mineralogical preservation state of enamel ideally by spatially resolved in-situ techniques such as Raman and LA-(MC)-ICP-MS. By analysing profiles across the enamel, the least altered zones can be identified and sampled from fossil tooth specimens. This is especially important for the application of non-traditional stable isotope systems such as $\delta^{44}Ca$, $\delta^{88}Sr$, $\delta^{26}Mg$ and $\delta^{64}Zn$ values used as trophic level indicators for the reconstruction of fossil food chains (Knudson et al., 2010; Jaouen and Pons, 2017; Martin et al., 2015, 2017; Bourgon et al., 2020). For these isotopes displaying trophic level differences in the sub-permil range, even small degrees of diagenetic alteration can strongly bias original compositions. Due to the experimental setup of this study, it is not possible to evaluate differences in the isotopic behaviour within a specific element, due to the high concentration of different element systems in the tracer solution. To better understand the differences between heavier and lighter isotopes during 90 °C, another experimental and analytical setup would be necessary, i.e. by using single element solutions with reduced isotopic concentration gradients (i.e. only near-natural isotopic enrichment). The experiment as presented in this study lack of some limitations regarding the application to natural post-mortem alteration processes, especially due to the high concentration of the doped isotopes, the composition of the aqueous solution in general and the lack of sediment. To overcome these limitations independent experiments to evaluate isotopic fractionation effects during dissolution and/or precipitation of hydroxylapatite should be performed. Single element solutions with and without sediment should be used at different temperatures, using high-resolution analytical techniques, such as MC-ICP-MS or TIMS, to further assess changes in the isotopic composition in the per mil range, which is relevant for palaeoecological and palaeoenvironmental applications using isotope compositions of fossil teeth.

5. Conclusion

In general, low, near Earth-surface temperatures (30 °C) do not affect the chemical alteration of dental tissues in acidic aqueous solution as much as higher temperatures of 90 °C (representing about 3 km of burial depth). Enamel isotope composition and apatite crystallinity are both much less affected by the in-vitro alteration experiment in the isotopically enriched tracer solution than in dentin. The isotopic ratios of dentin are fully altered at 90 °C after only few days. Calcium, Mg, Zn and Sr concentrations and isotopic compositions indicate that only the outermost ≈ 100–200 μm of the enamel are affected by reaction processes, probably diffusion and re-precipitation. High-resolution in-situ LA-MC-ICP-MS $^{87}Sr/^{86}Sr$ profiles across the dental cubes indicate that the central part of mm-thick enamel preserves original isotope compositions (even after 63 days at 90 °C), while dentin is fully altered after one week. This finding has implications for only few 100 μm thick enamel of certain fossil reptiles or small vertebrates. To measure pristine, in-vivo isotope compositions, we recommend to either remove the outermost ≈ 100–200 μm of enamel, as well as not to sample too close to the EDJ, or work with spatially resolving methods such as SIMS or laser ablation (MC-)ICP-MS to identify and avoid diagenetically altered zones. Magnesium and Zn show a different behaviour than Ca and Sr during the experimental bioapatite alteration. Zinc is incorporated into the dentin, while Mg is leached out of the dentin. The incorporation of Zn into the hydroxylapatite could be the reason for a decreasing Raman shift, causing the precipitation of crystals with less structural defects. Due to the lack of correlation between the reaction depth of the apatite (i.e. changes in isotope ratio and Raman spectra) and the duration of the experiments, it is not possible to determine the kinetic mechanism causing the alteration reaction. In contrast, it was possible to explain the different evolutions for the doped isotopes of Sr and Ca during the 90 °C experiment in the alteration zones of the bioapatite. A diffusion gradient-controlled mechanism at the solid/liquid interface around the dental cubes due to the highly elevated concentration of the doped isotopes likely caused the altered isotope ratios in the outer few 100 μm enamel and throughout the dentin.

Human rights

This article does not contain any studies with human subjects performed by the any of the authors.

Animal studies

This article does not contain any studies with animal subjects performed by the any of the authors.

Declaration of competing interest

The authors declare that they have no conflict of interest.

Acknowledgement

This project has received funding from the European Research Council (ERC) under the European Union's Horizon 2020 research and innovation programme (grant agreement No 681450) and the DFG grant nr. TU 148/9-1. This is contribution 30 of the DFG-funded research unit FOR 2685 "The Limits of the Fossil Record: Analytical and Experimental Approaches to Fossilization". We also acknowledge funding by the Max-Planck Graduate Center. We thank Alexander Gehler (University of Göttingen) who kindly supplied the tooth fragments of the African elephant molar (AG-Lox) from which dental cubes were cut and used for the alteration experiments. We thank Klaus Peter Jochum (Max-Planck Institute for Chemistry, Mainz) for the access to the LA-MC-ICP-MS laboratory.

Appendix A. Supplementary data

Supplementary data to this article can be found online at https://doi.org/10.1016/j.chemgeo.2021.120196.

References

Armstrong, J.T., 1995. Citzaf-a package of correction programs for the quantitative Electron Microbeam X-Ray-Analysis of thick polished materials, thin-films, and particles. Microbeam Anal. 4, 177–200.

Asjadi, F., Geisler, T., Salahi, I., Euler, H., Mobasherpour, I., 2019. Ti-substituted hydroxylapatite precipitated in the presence of titanium sulphate: a novel photocatalyst? Am. J. Chem. Appl. 6, 1–10.

Aufort, J., Gervais, C., Segalen, L., Labourdette, N., Coelho-Diogo, C., Baptiste, B., Beyssac, O., Amiot, R., Lécuyer, C., Balan, E., 2019. Atomic scale transformation of bone in controlled aqueous alteration experiments. Palaeogeogr. Palaeoclimatol. Palaeoecol. 526, 80–95.
Ayliffe, L.K., Chivas, A.R., Leakey, M.G., 1994. The retention of primary oxygen isotope compositions of fossil elephant skeletal phosphate. Geochim. Cosmochim. Acta 58, 5291–5298.
Barthel, H.J., Fougerouse, D., Geisler, T., Rust, J., 2020. Fluoridation of a lizard bone embedded in Dominican amber suggests open-system behavior. PLoS One 15, e0228843.
Beasley, D.E., Koltz, A.M., Lambert, J.E., Fierer, N., Dunn, R.R., 2015. The evolution of stomach acidity and its relevance to the human microbiome. PLoS One 10, e0134116.
Berkovitz, B.K., Shellis, R.P., 2016. The Teeth of Non-mammalian Vertebrates. Academic Press, London, San Diego, Cambridge, p. 342.
Berkovitz, B.K., Shellis, R.P., 2018. The Teeth of Mammalian Vertebrates (Pp.334). Academic Press, London, San Diego, Cambridge.
Berna, F., Matthews, A., Weiner, S., 2004. Solubilities of bone mineral from archaeological sites: the recrystallization window. J. Archaeol. Sci. 31, 867–882.
Boanini, E., Gazzano, M., Bigi, A., 2010. Ionic substitutions in calcium phosphates synthesized at low temperature. Acta Biomater. 6, 1882–1894.
Bocherens, H., Brinkman, D.B., Dauphin, Y., Mariotti, A., 1994. Microstructural and geochemical investigations on Late Cretaceous archosaur teeth from Alberta, Canada. Can. J. Earth Sci. 31, 783–792.
Bourgon, N., Jaouen, K., Bacon, A.M., Jochum, K.P., Dufour, E., Duringer, P., Ponche, J. L., Joannes-Boyau, R., Boesch, Q., Antoine, P.O., Hullot, M., Weis, U., Schulz-Kornas, E., Trost, M., Fiorillo, D., Demeter, F., Patole-Edoumba, E., Shackelford, L.L., Dunn, T.E., Zachwieja, A., Duangthongchit, S., Sayavonkhamdy, T., Sichanthongtip, P., Sihanam, D., Souksavatdy, V., Hublin, J.J., Tütken, T., 2020. Zinc isotopes in Late Pleistocene fossil teeth from a Southeast Asian cave setting preserve paleodietary information. Proc. Nat. Acad. Sci. USA 117, 4675–4681.
Budd, P., Montgomery, J., Barreiro, B., Thomas, R.G., 2000. Differential diagenesis of strontium in archaeological human dental tissues. Appl. Geochem. 15, 687–694.
Chander, S., Fuerstenau, D.W., 1984. Solubility and interfacial properties of hydroxylapatite: a review. In: Adsorption on and Surface Chemistry of Hydroxylapatite. Springer, Boston, pp. 29–49.
Clarke, A.D., Telmer, K.H., Mark Shrimpton, J., 2007. Elemental analysis of otoliths, fin rays and scales: a comparison of bony structures to provide population and life-history information for the Arctic grayling (*Thymallus arcticus*). Ecol. Freshw. Fish 16, 354–361.
Clementz, M.T., Holden, P., Koch, P.L., 2003. Are calcium isotopes a reliable monitor of trophic level in marine settings? Int. J. Osteoarchaeol. 13, 29–36.
Copeland, S.R., Sponheimer, M., Lee-Thorp, J.A., le Roux, P.J., de Ruiter, D.J., Richards, M.P., 2010. Strontium isotope ratios in fossil teeth from South Africa: assessing laser ablation MC-ICP-MS analysis and the extent of diagenesis. J. Archaeol. Sci. 37, 1437–1446.
DeNiro, M.J., Epstein, S., 1978. Influence of diet on the distribution of carbon isotopes in animals. Geochim. Cosmochim. Acta 25, 495–506.
DeNiro, M.J., Epstein, S., 1981. Influence of diet on the distribution of nitrogen isotopes in animals. Geochim. Cosmochim. Acta 45, 341–351.
DePaolo, D.J., 2011. Surface kinetic model for isotopic and trace element fractionation during precipitation of calcite from aqueous solutions. Geochim. Cosmochim. Acta 75, 1039–1056.
Dorozhkin, S.V., 2012. Dissolution mechanism of calcium apatites in acids: a review of literature. World J. Methodol. 2, 1.
Ericson, J.E., 1985. Strontium isotope characterization in the study of prehistoric human ecology. J. Hum. Evol. 14, 503–514.
Fassbender, H.W., Lin, H.C., Ulrich, B., 1966. Löslichkeit und Löslichkeitsprodukt von Hydroxylapatit und Rohphosphaten. Zeitschrift für Pflanzenernährung, Düngung, Bodenkunde 112, 101–113.
Featherstone, J.D.B., Nelson, D.G.A., 1980. The effect of fluoride, zinc, strontium, magnesium and iron on the crystal-structural disorder in synthetic carbonated apatites. Aust. J. Chem. 33, 2363–2368.
Galy, A., Belshaw, N.S., Halicz, L., O'Nions, R.K., 2001. High-precision measurement of magnesium isotopes by multiple-collector inductively coupled plasma mass spectrometry. Int. J. Mass Spectrom. 208, 89–98.
Garçon, M., Sauzeat, L., Carlson, R.W., Shirey, S.B., Simon, M., Balter, V., Boyet, M., 2017. Nitrile, latex, neoprene and vinyl gloves: a primary source of contamination for trace element and Zn isotopic analyses in geological and biological samples. Geostand. Geoanal. Res. 41, 367–380.
Gehler, A., Tütken, T., Pack, A., 2012. Oxygen and carbon isotope variations in a modern rodent community–implications for palaeoenvironmental reconstructions. PLoS One 7 (11), e49531.
Hedges, R.E.M., 2002. Bone diagenesis: an overview of processes. Archaeometry 44, 319–328.
Hedges, R.E.M., Millard, A.R., Pike, A.W.G., 1995. Measurements and relationships of diagenetic alteration of bone from three archaeological sites. J. Archaeol. Sci. 22, 201–209.
Heuser, A., Tütken, T., Gussone, N., Galer, S.J.G., 2011. Calcium isotopes in fossil bones and teeth-Diagenetic versus biogenic origin. Geochim. Cosmochim. Acta 75, 3419–3433.
Hillson, S., 2005. Teeth, 2nd edition. Cambridge University Press, Cambridge. 373 pp.
Hinz, E.A., Kohn, M.J., 2010. The effect of tissue structure and soil chemistry on trace element uptake in fossils. Geochim. Cosmochim. Acta 74, 3213–3231.
Hoppe, K.A., Koch, P.L., Carlson, R.W., Webb, S.D., 1999. Tracking mammoths and mastodons: reconstruction of migratory behavior using strontium isotope ratios. Geology 27, 439–442.
Hoppe, K.A., Koch, P.L., Furutani, T.T., 2003. Assessing the preservation of biogenic strontium in fossil bones and tooth enamel. Int. J. Osteoarchaeol. 13, 20–28.
Horstwood, M.S.A., Evans, J.A., Montgomery, J., 2008. Determination of Sr isotopes in calcium phosphates using laser ablation inductively coupled plasma mass spectrometry and their application to archaeological tooth enamel. Geochim. Cosmochim. Acta 72, 5659–5674.
Ingle, C.P., Sharp, B.L., Horstwood, M.S.A., Parrish, R.R., Lewis, D.J., 2003. Instrument response functions, mass bias and matrix effects in isotope ratio measurements and semi-quantitative analysis by single and multi-collector ICP-MS. J. Anal. At. Spectrom. 18, 219–229.
Inskeep, W.P., Silvertooth, J.C., 1988. Kinetics of hydroxylapatite precipitation at pH 7.4 to 8.4. Geochim. Cosmochim. Acta 52, 1883–1893.
Irrgeher, J., Galler, P., Prohaska, T., 2016. $^{87}Sr/^{86}Sr$ isotope ratio measurements by laser ablation multicollector inductively coupled plasma mass spectrometry: Reconsidering matrix interferences in bioapatites and biogenic carbonates. Spectrochim. Acta Part B Atom. Specrosc. 125, 31–42.
Jaouen, K., Pons, M.L., 2017. Potential of non-traditional isotope studies for bioarchaeology. Archaeol. Anthropol. Sci. 9, 1389–1404.
Jaouen, K., Pons, M.-L., Balter, V., 2013. Iron, copper and zinc isotopic fractionation up mammal trophic chains. Earth Planet. Sci. Lett. 374, 164–172.
Jaouen, K., Szpak, P., Richards, M.P., 2016a. Zinc isotope ratios as indicators of diet and trophic level in arctic marine mammals. PLoS One 11, e0152299.
Jaouen, K., Beasley, M., Schoeninger, M., Hublin, J.J., Richards, M.P., 2016b. Zinc isotope ratios of bones and teeth as new dietary indicators: results from a modern food web (Koobi Fora, Kenya). Sci. Rep. 6, 26281.
Jaouen, K., Trost, M., Bourgon, N., Colleter, R., Le Cabec, A., Tütken, T., Elias Oliveira, R., Pons, M.L., Méjean, P., Steinbrenner, S., Chmeleff, J., 2020. Zinc isotope variations in archeological human teeth (Lapa do Santo, Brazil) reveal dietary transitions in childhood and no contamination from gloves. PLoS One 15, e0232379.
Jochum, K.P., Nohl, L., Herwig, K., Lammel, E., Stoll, B., Hofmann, A.W., 2005. GeoReM: a new geochemical database for reference materials and isotopic standards. Geostand. Geoanal. Res. 29, 333–338.
Jochum, K.P., Stoll, B., Herwig, K., Willbold, M., 2007. Validation of LA-ICP-MS trace element analysis of geological glasses using a new solid-state 193 nm Nd: YAG laser and matrix-matched calibration. J. Anal. At. Spectrom. 22, 112–121.
Keenan, S.W., Engel, A.S., 2017. Early diagenesis and recrystallization of bone. Geochim. Cosmochim. Acta 196, 209–223.
Knudson, K.J., Williams, H.M., Buikstra, J.E., Tomczak, P.D., Gordon, G.W., Anbar, A.D., 2010. Introducing $\delta^{88/86}Sr$ analysis in archaeology: a demonstration of the utility of strontium isotope fractionation in paleodietary studies. J. Archaeol. Sci. 37, 2352–2364.
Koch, P.L., Tuross, N., Fogel, M.L., 1997. The effects of sample treatment and diagenesis on the isotopic integrity of carbonate in biogenic hydroxylapatite. J. Archaeol. Sci. 24, 417–429.
Kohn, M.J., Moses, R.J., 2013. Trace element diffusivities in bone rule out simple diffusive uptake during fossilization but explain in vivo uptake and release. Proc. Natl. Acad. Sci. 110, 419–424.
Kohn, M.J., Schoeninger, M.J., Barker, W.B., 1999. Altered states: Effects of diagenesis on fossil tooth chemistry. Geochim. Cosmochim. Acta 63, 2737–2747.
Lee-Thorp, J., van der Merwe, N., Brain, C.K., 1989. Isotopic evidence for dietary differences between two extinct baboon species from Swartkrans. J. Hum. Evol. 18, 183–189.
Lee-Thorp, J., Thackeray, J.F., van der Merwe, N., 2000. The hunters and the hunted revisited. J. Hum. Evol. 39, 565–576.
LeGeros, R.Z., Sakae, T., Bautista, C., Retino, M., LeGeros, J.P., 1996. Magnesium and carbonate in enamel and synthetic apatites. Adv. Dent. Res. 10, 225–231.
Lewis, J., Coath, C.D., Pike, A.W.G., 2014. An improved protocol for $^{87}Sr/^{86}Sr$ by laser ablation multi-collector inductively coupled plasma mass spectrometry using oxide reduction and a customised plasma interface. Chem. Geol. 390, 173–181.
Lewis, J., Pike, A.W.G., Evershed, R.P., 2017. Strontium concentration, radiogenic ($^{87}Sr/^{86}Sr$) and stable ($\delta^{88}Sr$) strontium isotope systematics in a controlled feeding study. STAR 3, 45–57.
Lugli, F., Cipriani, A., Peretto, C., Mazzucchelli, M., Brunelli, D., 2017. In situ high spatial resolution $^{87}Sr/^{86}Sr$ ratio determination of two Middle Pleistocene (c.a. 580 ka) *Stephanorhinus hundsheimensis* teeth by LA–MC–ICP–MS. Int. J. Mass Spectrom. 412, 38–48.
MacFadden, B.J., DeSantis, L.R., Hochstein, J.L., Kamenov, G.D., 2010. Physical properties, geochemistry, and diagenesis of xenarthran teeth: prospects for interpreting the paleoecology of extinct species. Palaeogeography, Palaeoclimatology, Palaeoecology 291 (3-4), 180–189.
Martin, J.E., Vance, D., Balter, V., 2014. Natural variation of magnesium isotopes in mammal bones and teeth from two South African trophic chains. Geochim. Cosmochim. Acta 130, 12–20.
Martin, J.E., Vance, D., Balter, V., 2015. Magnesium stable isotope ecology using mammal tooth enamel. Proc. Nat. Acad. Sci. USA 112, 430–435.
Martin, J.E., Tacail, T., Balter, V., 2017. Non-traditional isotope perspectives in vertebrate palaeobiology. Palaeontology 60, 485–502.
Mayer, I., Featherstone, J.D.B., 2000. Dissolution studies of Zn-containing carbonated hydroxylapatites. J. Cryst. Growth 219, 98–101.
McArthur, J.M., Howarth, R.J., Bailey, T.R., 2001. Strontium isotope stratigraphy: LOWESS version 3: best fit to the marine Sr-isotope curve for 0–509 Ma and accompanying look-up table for deriving numerical age. J. Geol. 109, 155–170.

Meija, J., Coplen, T.B., Berglund, M., Brand, W.A., De Bièvre, P., Gröning, M., Holden, N. E., Irrgeher, J., Loss, R.D., Walczyk, T., Prohaska, T., 2016. Atomic weights of the elements 2013 (IUPAC Technical Report). Pure and Applied Chemistry 88 (3), 265–291.
Melin, A.D., Crowley, B.E., Brown, S.T., Wheatley, P.V., Moritz, G.L., Yit Yu, F.T., Bernard, H., DePaolo, D.J., Jacobson, A.D., Dominy, N.J., 2014. Calcium and carbon stable isotope ratios as paleodietary indicators. Am. J. Phys. Anthropol. 154, 633–643.
Mischel, S.A., Mertz-Kraus, R., Jochum, K.P., Scholz, D., 2017. TERMITE: an R script for fast reduction of laser ablation inductively coupled plasma mass spectrometry data and its application to trace element measurements. Rapid Commun. Mass Spectrom. 31, 1079–1087.
Müller, W., Nava, A., Evans, D., Rossi, P.F., Alt, K.W., Bondioli, L., 2019. Enamel mineralization and compositional time-resolution in human teeth evaluated via histologically-defined LA-ICPMS profiles. Geochim. Cosmochim. Acta 255, 105–126.
Munro, L.E., Longstaffe, F.J., White, C.D., 2007. Burning and boiling of modem deer bone: Effects on crystallinity and oxygen isotope composition of bioapatite phosphate. Palaeogeogr. Palaeoclimatol. Palaeoecol. 249, 90–102.
Nelson, D.G.A., Featherstone, J.D.B., Duncan, J.F., Cutress, T.W., 1982. Paracrystalline disorder of biological and synthetic carbonate-substituted apatites. J. Dent. Res. 61, 1274–1281.
Pasteris, J.D., Ding, D.Y., 2009. Experimental fluoridation of nanocrystalline apatite. Am. Mineral. 94, 53–63.
Pasteris, J.D., Yoder, C.H., Wopenka, B., 2014. Molecular water in nominally unhydrated carbonated hydroxylapatite: the key to a better understanding of bone mineral. Am. Mineral. 99, 16–27.
Pearce, E.I.F., 1988. On the dissolution of hydroxylapatite in acid solutions. J. Dent. Res. 67, 1056–1058.
Person, A., Bocherens, H., Saliège, J.F., Paris, F., Zeitoun, V., Gérard, M., 1995. Early diagenetic evolution of bone phosphate: an X-ray diffractometry analysis. Journal of Archaeological Science 22 (2), 211–221.
Pfretzschner, H.-U., 2004. Fossilization of Haversian bone in aquatic environments. Comptes Rendus Palevol. 3, 605–616.
Popović, L., De Waal, D., Boeyens, J.C.A., 2005. Correlation between Raman wavenumbers and P-O bond lengths in crystalline inorganic phosphates. J. Raman Spectrosc. 36, 2–11.
Potasznik, A., Szymczyk, S., 2015. Magnesium and calcium concentrations in the surface water and bottom deposits of a river-lake system. J. Elem. 20.
Price, T.D., Johnson, C.M., Ezzo, J.A., Ericson, J., Burton, J.H., 1994. Residential mobility in the prehistoric Southwest United States: a preliminary study using strontium isotope analysis. J. Archaeol. Sci. 21, 315–330.
Pucéat, E., Reynard, B., Lécuyer, C., 2004. Can crystallinity be used to determine the degree of chemical alteration of biogenic apatites? Chem. Geol. 205, 83–97.
Reiche, I., Favre-Quattropani, L., Vignaud, C., Bocherens, H., Charlet, L., Menu, M., 2003. A multi-analytical study of bone diagenesis: the Neolithic site of Bercy (Paris, France). Meas. Sci. Technol. 14, 1608–1619.
Saloman, E.B., 2006. Wavelengths, energy level classifications, and energy levels for the spectrum of neutral mercury. J. Phys. Chem. Ref. Data 35, 1519–1548.
Schweitzer, M.H., Marshall, M., Carron, K., Bohle, D.S., Busse, S.C., Arnold, E.V., Barnard, D., Horner, J.R., Starkey, J.R., 1997. Heme compounds in dinosaur trabecular bone. Proceedings of the National Academy of Sciences 94 (12), 6291–6296.
Schoeninger, M.J., Hallin, K., Reeser, H., Valley, J.W., Fournelle, J., 2003. Isotopic alteration of mammalian tooth enamel. Int. J. Osteoarchaeol. 13, 11–19.
Shalev, N., Gavrieli, I., Halicz, L., Sandler, A., Stein, M., Lazar, B., 2017. Enrichment of ^{88}Sr in continental waters due to calcium carbonate precipitation. Earth Planet. Sci. Lett. 459, 381–393.
Sillen, A., Hall, G., Armstrong, R., 1995. Strontium/calcium ratios (Sr/Ca) and strontium isotopic ratios ($^{87}Sr/^{86}Sr$) of *Australopithecus robustus* and *Homo* sp. from Swartkrans. J. Hum. Evol. 28, 277–285.
Simonetti, A., Buzon, M.R., Creaser, R.A., 2008. In-situ elemental and Sr isotope investigation of human tooth enamel by Laser Ablation-(MC-)ICP-MS: Successes and pitfalls. Archaeometry 50, 371–385.
Skulan, J., DePaolo, D.J., Owens, T.L., 1997. Biological control of calcium isotopic abundances in the global calcium cycle. Geochim. Cosmochim. Acta 61, 2505–2510.
Snoeck, C., Lee-Thorp, J., Schulting, R., de Jong, J., Debouge, W., Mattielli, N., 2015. Calcined bone provides a reliable substrate for strontium isotope ratios as shown by an enrichment experiment. Rapid Commun. Mass Spectrom. 29, 107–114.
Sponheimer, M., Lee-Thorp, J.A., 2006. Enamel diagenesis at South African Australopith sites: Implications for paleoecological reconstruction with trace elements. Geochim. Cosmochim. Acta 70, 1644–1654.
Stiner, M.C., Kuhn, S.L., 1995. Differential burning, recrystallization, and fragmentation of archaeological bone. J. Archaeol. Sci. 22, 223–237.
Suarez, C.A., Kohn, M.J., 2020. Caught in the act: a case study on microscopic scale physicochemical effects of fossilization on stable isotopic composition of bone. Geochim. Cosmochim. Acta 268, 277–295.
Tacail, T., Albalat, E., Télouk, P., Balter, V., 2014. A simplified protocol for measurement of Ca isotopes in biological samples. J. Anal. At. Spectrom. 29, 529–535.
Tacail, T., Le Houedec, S., Skulan, J.L., 2020. New frontiers in calcium stable isotope geochemistry: perspectives in present and past vertebrate biology. Chem. Geol. 537, 119471.
Tanabe, K., Hiraishi, J., 1980. Correction of finite slit width effects on Raman line widths. Spectrochim. Acta 36, 341–344.
Thomas, D.B., Fordyce, R.E., Frew, R.D., Gordon, K.C., 2007. A rapid, non-destructive method of detecting diagenetic alteration in fossil bone using Raman spectroscopy. J. Raman Spectrosc. 38, 1533–1537.
Thomas, D.B., McGoverin, C.M., Fordyce, R.E., Frew, R.D., Gordon, K.C., 2011. Raman spectroscopy of fossil bioapatite — a proxy for diagenetic alteration of the oxygen isotope composition. Palaeogeogr. Palaeoclimatol. Palaeoecol. 310, 62–70.
Tütken, T., Vennemann, T.W., 2011. Fossil bones and teeth: preservation or alteration of biogenic compositions? Palaeogeogr. Palaeoclimatol. Palaeoecol. 310, 1–8.
Vennemann, T.W., Hegner, E., Cliff, G., Benz, G.W., 2001. Isotopic composition of recent shark teeth as a proxy for environmental conditions. Geochim. Cosmochim. Acta 65, 1583–1599.
Vroon, P.Z., Van Der Wagt, B., Koornneef, J.M., Davies, G.R., 2008. Problems in obtaining precise and accurate Sr isotope analysis from geological materials using laser ablation MC-ICPMS. Anal. Bioanal. Chem. 390, 465–476.
Wang, Y., Cerling, T.E., 1994. A model of fossil tooth and bone diagenesis: implications for paleodiet reconstruction from stable isotopes. Palaeogeogr. Palaeoclimatol. Palaeoecol. 107, 281–289.
Weber, M., Wassenburg, J.A., Jochum, K.P., Breitenbach, S.F.M., Oster, J., Scholz, D., 2017. Sr-isotope analysis of speleothems by LA-MC-ICP-MS: high temporal resolution and fast data acquisition. Chem. Geol. 468, 63–74.
Weber, M., Lugli, F., Jochum, K.P., Cipriani, A., Scholz, D., 2018. Calcium carbonate and phosphate reference materials for monitoring bulk and microanalytical determination of Sr isotopes. Geostand. Geoanal. Res. 42, 77–89.
Weber, M., Lugli, F., Hattendorf, B., Scholz, D., Mertz-Kraus, R., Guinoiseau, D., Jochum, K.P., 2020a. NanoSr – a new carbonate microanalytical reference material for in situ strontium isotope analysis. Geostand. Geoanal. Res. 44, 69–83.
Weber, M., Tacail, T., Lugli, F., Clauss, M., Weber, K., Leichliter, J., Winkler, D.E., Mertz-Kraus, R., Tütken, T., 2020b. Strontium uptake and intra-population $^{87}Sr/^{86}Sr$ variability of bones and teeth–controlled feeding experiments with rodents (*Rattus norvegicus, Cavia porcellus*). Front. Ecol. Evol. 8, 434.
Wieser, M.E., Buhl, D., Bouman, C., Schwieters, J., 2004. High precision calcium isotope ratio measurements using a magnetic sector multiple collector inductively coupled plasma mass spectrometer. J. Anal. At. Spectrom. 19, 844–851.
Zazzo, A., Lécuyer, C., Mariotti, A., 2004a. Experimentally controlled carbon and oxygen isotope exchange between bioapatites and water under inorganic and microbially-mediated conditions. Geochim. Cosmochim. Acta 68, 1–12.
Zazzo, A., Lécuyer, C., Sheppard, S.M.F., Grandjean, P., Mariotti, A., 2004b. Diagenesis and the reconstruction of paleoenvironments: a method to restore original $\delta^{18}O$ values of carbonate and phosphate from fossil tooth enamel. Geochim. Cosmochim. Acta 68, 2245–2258.
Zhu, Z.Y., Jiang, S.Y., Yang, T., Wei, H.Z., 2015. Improvements in Cu–Zn isotope analysis with MC-ICP-MS: a revisit of chemical purification, mass spectrometry measurement and mechanism of Cu/Zn mass bias decoupling effect. Int. J. Mass Spectrom. 393, 34–40.